Regular Article

The effect of fins and wavy geometry on natural convection heat transfer of TiO$_2$–water nanofluid in trash bin-shaped cavity

Jalil Fereidooni[a]

Department of Mechanical Engineering, Malek-Ashtar University of Technology, Shahin Shahr, Iran

Abstract This paper studies the effect of fins number and size and wavy wall of a trash bin-shaped cavity on the natural convection heat transfer (NC) of a TiO$_2$–water nanofluid. The flow is considered buoyancy driven, which is under thermal radiation. The effects of Rayleigh number ($10^3 - 10^5$), thermal radiation ($0.1-0.3$), nanoparticle concentration ($0.02-0.04$), and geometry are investigated. Non-dimensional mode of NS equations would be governing equations, and the finite element technique is utilized to discrete them. Two plans are examined: firstly, the effects of thermal parameters on the enclosure with no fin are studied. Secondly, the effects of the fins length and number, and also the wavy geometry on Nusselt number (Nu) and flow distribution are investigated. The findings of the present paper are that increasing the fin number around the inner cylinder increases Nu$_{avg}$ up to 54%, and reduces the local entropy generation (EG) and enhances the Bejan number. Moreover, if the wavy wall amplitude changes from 0.05 to 0.1, Nu$_{avg}$ reduces by 31%, and if the Ra changes from 10^3 to 10^5, Nu$_{avg}$ increases up to 36%.

List of symbols

ψ	Stream function
Nu	Nusselt number
ρ	Density
μ	Dynamic viscosity
β	Volume expansion coefficient
Pr	Prandtl number
ϕ	Nanoparticle volume fraction
T	Temperature
S	Entropy generation
Rd	Radiation parameter
Ra	Rayleigh number
L	Length of cavity

Subscripts

nf	Nanofluid
c	Cold
loc.	Local
ave.	Average

[a] e-mail: j.fereidooni@gmail.com (corresponding author)

1 Introduction

Adding nanoparticles laden in base fluids is a novel method for enhancing heat transfer. This idea was firstly introduced by Choi and Eastman [1]. This method is applicable in different branches of science and engineering such as HVAC [2], heat exchangers [3,4], solar energy [5], heat pipe [6,7], blood flow [8,9], and composites [10,11]. The effects of various parameters, namely, Rayleigh number, Hartmann number, radiation, and also different shapes of cavities, are investigated by researchers.

The effect of geometry is one of the most critical factors in natural convection (NC) analysis. Disparate structures of chamber, i.e., rectangular [12], triangle-shaped [13], trapezoid-shaped [14], and unusual forms are perused. Bahiraei et al. studied hybrid nanofluid of graphene and silver in a microchannel heat sink with ribs which directed the flow toward secondary channels. They concluded that the average convective heat transfer coefficient has a direct relation with Reynolds number and the concentration of nanoparticles [15]. Sun and pop analyzed NC in a triangle-shaped cavity. Three types of nanomaterials were applied to explore the mean Nusselt number and temperature features [16]. Ashorynejad and Hoseinpour studied NC in a porous chamber. They used lattice Boltzmann method (LBM) to calculate entropy generation and average Nusselt number [17]. Eshaghi et al. [18] studied FEM simula-

tion of double-diffusive NC in an H-shaped chamber. Besides, they investigated the effect of varying configuration of fin on the flow. Bahmani et al. [19] studied turbulent heat transfer of a water–alumina nanofluid in a double pipe heat exchanger. They solved the governing equations by the finite volume method and studied the effects of Reynolds number, nanoparticle volume fraction, and flow direction on Nusselt number and thermal efficiency. They reached 32.7% enhancement in Nusselt number by changing the mentioned parameters. Hatami et al. studied NC heat transfer in circular and wavy cavity. They used RSM to detect the best geometry for the wavy wall and also RSM and FEM for optimizing the results. The best case (between the tested cases) is when the number of the undulations is 12 and the amplitude value is 0.3. Their proposed method had a widespread application in time-efficient optimization of heat transfer in irregular geometries [20]. The effect of wavy wall is another interesting parameter studied in literature. Few studies conducted this issue in their analysis. Abdelkaber et al. [21] studied the effect of different aspect ratios of the wavy wall on Nusselt number in various Ra numbers. Nguyen et al. [22] did the numerical study about the interaction of wavy nanofluid and porous media enclosure on the NC for Cu–water nanofluid. They used the ISPH method to solve their governing equations. Various ranges of Rayleigh number ($10^3 - 10^6$), Darcy ($10^{-6} - 10^{-1}$), and porous medium height ($0.25-0.75$), amplitude ($0-0.25$), and undulation number ($1-3$) were considered in their work. Waqas et al. [23] studied the theoretical analysis of the SWCNT–MWCNT in a rotating disk using von Karman approach. Rao et al. [24] studied the NC of a heat source which was embedded in a wavy cavity. The effect of various parameters such as heater's non-dimensional length and waviness of the right wall were investigated. They concluded that non-dimensional length reduces the rate of convection. Dogonchi et al. [25] did a numerical investigation on NC of Cu–water nanofluid in a square wavy cavity. They used CVFEM to solve the governing equations, and their most important finding was that wavy contraction ratio has a negative impact on NC heat transfer. The effect of the shape of the nanoparticles was also considered by Dogonchi et al. [26]. They used irregular triangular enclosure for their analysis. Other related works can be found in Refs. [27–35].

The effect of fin's number and shape on the heat transfer is an ongoing topic that is popular among researchers in the field of heat transfer. Feng et al. [36] studied two series of fins in a new cross-fin heat sink: perpendicular short fins and long fins. Their ultimate goal was to enhance natural convection heat transfer by considering both NC and radiation. They concluded that heat sink enhances both NC and radiation by 11% and 15%, respectively. It is vital to mention that they used both numerical and experimental analysis to validate their results. Saleh et al. [37] numerically studied the effect of flexible fin on NC in a square cavity by putting the fin on the left wall. They used Brinkman–Forchheimer extended Darcy flow model and searched the effects of fin oscillation and elasticity on the overall

intensity of heat transfer and concluded that both oscillation and elasticity of fin have a positive impact up to 3.4% on heat transfer rate. The effect of fin's length and location in a wavy enclosure with Galerkin weighted residual finite element technique was studied by Asad et al. [38]. The lower and upper walls were considered to be wavy and the most important finding was that the fin length causes an increase in $\mathrm{Nu_{avg}}$. Khetib et al. [39] studied the effect of curved, inclined, and straight fins on NC and entropy of the nanofluid in a square cavity. They found that increasing the fin's angle and curvature have a positive impact on heat transfer rate and entropy generation. Alfarhani et al. [40] considered porous enclosure with two fins attached to the hot wall to see the changes in NC of Al_2O_3–water nanofluid. They studied the effect of Hartman number, magnetic field, Ra, and length of the fins and concluded that the fin's length is in direct relation with heat transfer rate. Other works on the effect of fin can be found in [41,42].

Entropy generation (S) demonstrates the irreversibility of the fluid flow. S in cavities with nanofluids is due to friction, fluid flow, porous media, and magnetic field. Tayebi et al. [43] studied the entropy production of a hybrid nanofluid in an elliptical cavity. One of their important findings was that the maximum amount of entropy was achieved for higher Rayleigh numbers and nanoparticle concentration. Li et al. [44] studied entropy generation in a square cavity exposed to constant magnetic field. Their results showed that radiation and nanoparticle concentration increase the entropy generation. The entropy generation of hybrid nanofluid [45], entropy generation of simple fluids [46, 47], and the effect of geometry on S [48] are the hot topics for this parameter. Chamkha et al. [49] investigated the thorough effect of magnetohydrodynamic mixed convection on the parameter of entropy generation. They used finite volume technique to numerically analyze the effect of constant magnetic field on entropy generation in a gamma-shaped cavity. They concluded that the main factor which causes considerable change in entropy generation is nanoparticle volume fraction. Tilehnoee et al. [50] studied the entropy generation in an incinerator cavity with wavy heater. They considered the effect of different parameters in two flow regimes: laminar and turbulent flow. They demonstrated that Ra and Da enhance the entropy generation in laminar flow; however, the Da has a negative impact on $\mathrm{Nu_{avg}}$ when the flow is turbulent. Tilehnoee et al. [51] measured the entropy generation of NEPCMs in a porous cavity. They used four different channels with three configurations for cooling purpose. Their findings include the direct impact of Ha on Bejan number, and also the negative impact of Ra on Bejan number. Other works on entropy generation can be found in [52–56].

According to the aforesaid published papers, there may be a lack of investigations of the simultaneous effect of wavy wall geometry and the number and shape of the fins on NC and S in cavities. There is a gap in the investigation of the simultaneous effect of wavy wall and fins on such a geometry which is applicable mostly

Eur. Phys. J. Spec. Top. (2022) 231:2713–2731

2715
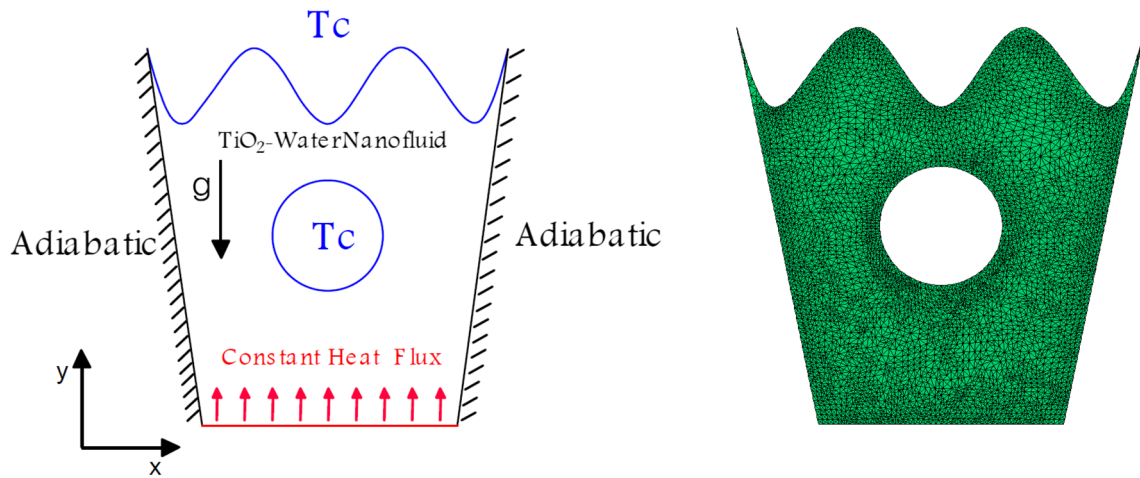
Fig. 1 Geometry of enclosure

in heat exchangers, valley due to sun radiator which is applied in studying the mechanism of fog, cooling appliances, building thermal elements, and thermal storage tanks. The present paper aims to investigate the effect of thermal parameters (Ra, Rd, and ϕ), and geometry on Nusselt number and S of TiO_2–water nanofluid in a wavy crown enclosure with a cylindrical obstacle inside. This is the first time that the effect of thermal and geometrical parameters on the NC and S is perused in this especial wavy container. This examination may be suitable in heat exchangers and their wavy walls, HVAC, and renewable energy systems such as solar energy systems with radiation effects.

2 Problem description

The geometry of the trash bin-shaped enclosure with a cylindrical obstacle inside may be depicted in Fig. 1. The mesh size and structure of the mesh is also shown in this figure. The boundary conditions are as follows: the right and left adiabatic walls, constant heat flux from the bottom wall, the cold top wavy wall, and the cold cylinder at the middle of the cavity. Boussinesq approximation is used for density changes, and there may be no slip condition among TiO_2 nanomaterials and water. Besides, the flow is at thermal equilibrium. Table 1 demonstrates the properties of TiO_2 and water.

The flow in this study is assumed incompressible, laminar, and steady. So, the governing equations would be [57,58]:

$$\frac{\partial u}{\partial x} + \frac{\partial v}{\partial y} = 0, \tag{1}$$

Table 1 Thermo-physical features of H_2O and TiO_2 [52]

	C_p	k	ρ
TiO_2	686.2	8.954	3250
H_2O	4179	0.613	997.1

Table 2 Comparison of Nu_{avg} of the present work and Oztop [66]

Ra_I	Ra_E	Present work	Oztop et al. [66]
10^4	10^4	1.39	1.36
10^5	10^5	3.74	3.79

$$u\frac{\partial u}{\partial x} + v\frac{\partial u}{\partial y} = -\frac{1}{\rho_{nf}}\frac{\partial p}{\partial x} + v_{nf}\left(\frac{\partial^2 u}{\partial x^2} + \frac{\partial^2 u}{\partial y^2}\right), \tag{2}$$

$$u\frac{\partial v}{\partial x} + v\frac{\partial v}{\partial y} = -\frac{1}{\rho_{nf}}\frac{\partial p}{\partial y} + v_{nf}\left(\frac{\partial^2 v}{\partial x^2} + \frac{\partial^2 v}{\partial y^2}\right)$$
$$+ \frac{(\rho\beta)_{nf}}{\rho_{nf}}g(T - T_c), \tag{3}$$

$$u\frac{\partial T}{\partial x} + v\frac{\partial T}{\partial y} = \frac{K_{nf}}{(\rho C_p)_{nf}}\left(\frac{\partial^2 T}{\partial x^2} + \frac{\partial^2 T}{\partial y^2}\right) - \frac{1}{(\rho C_p)_{nf}}\frac{\partial q_r}{\partial y}, \tag{4}$$

where $q_r = -\frac{4\sigma_r}{3\chi_r}\frac{\partial T^4}{\partial y}$ and $T^4 \cong -3T_c^4 + 4T_c^3 T$.
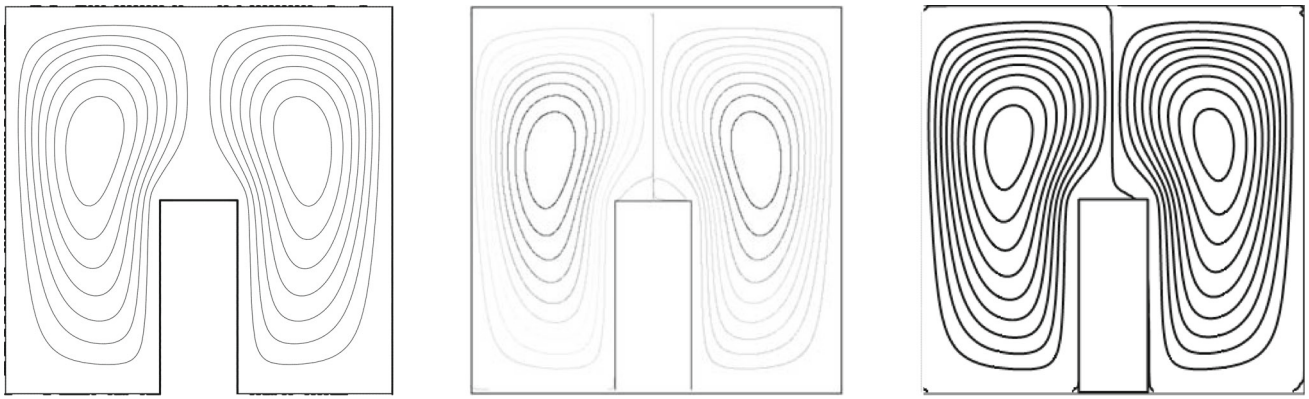
The following terms are introduced to make dimensionless mode of the above equations:

$$X = \frac{x}{L}, U = \frac{uL}{\alpha}, P = \frac{L^2 p}{\alpha_f^2 \rho_f},$$
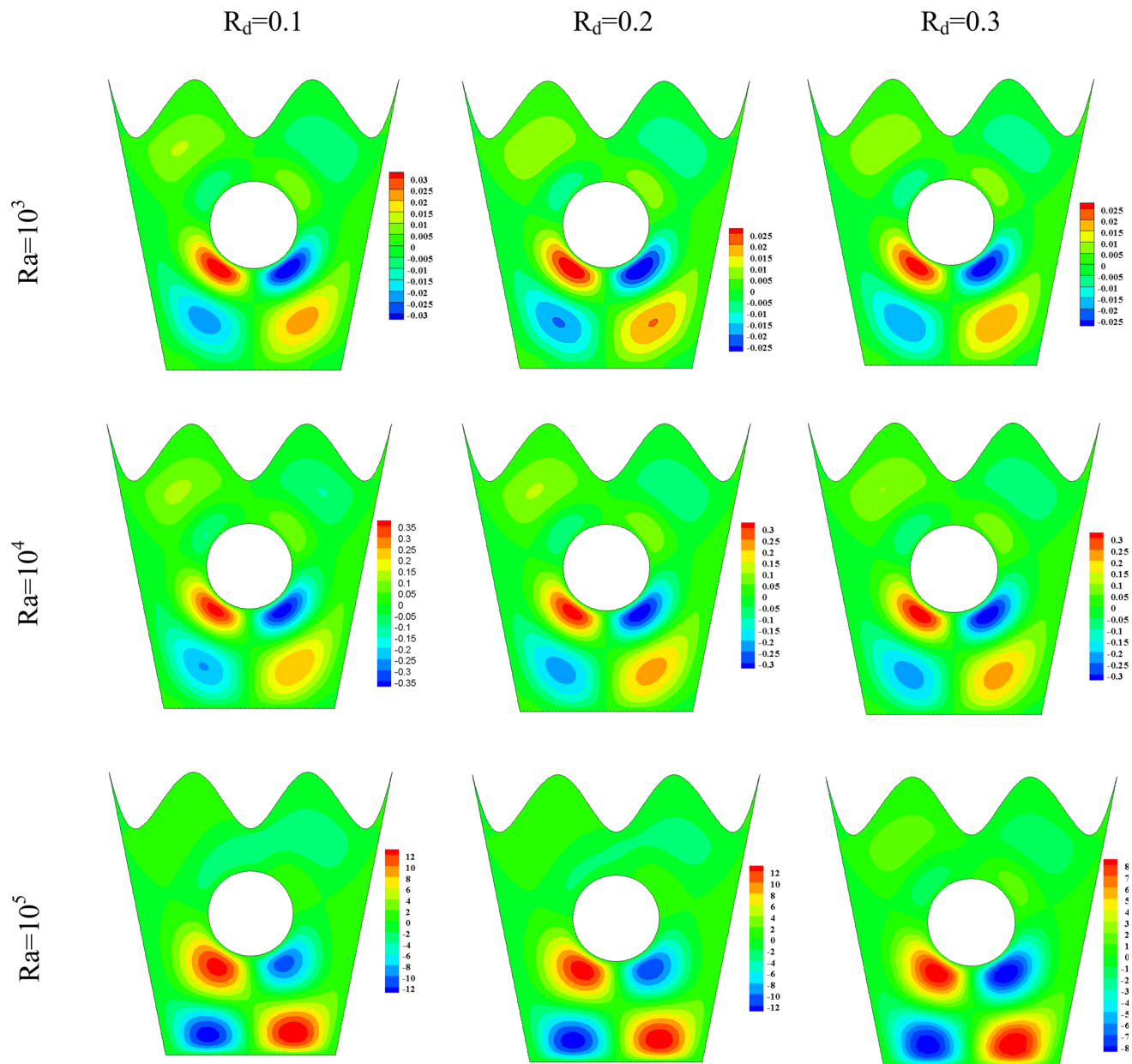$$Y = \frac{y}{L}, V = \frac{vL}{\alpha}, \theta = \frac{(T - T_c)}{\Delta T}. \tag{5}$$

Hence, Eqs. (1)–(4) may follow the following form:

$$U\frac{\partial U}{\partial X} + V\frac{\partial U}{\partial Y}$$
$$= -\frac{\rho_f}{\rho_{nf}}\frac{\partial P}{\partial X} + Pr\frac{(\mu_{nf}/\mu_f)}{(\rho_{nf}/\rho_f)}\left(\frac{\partial^2 U}{\partial X^2} + \frac{\partial^2 U}{\partial Y^2}\right), \tag{6}$$

$$U\frac{\partial V}{\partial X} + V\frac{\partial V}{\partial Y} = -\frac{\rho_f}{\rho_{nf}}\frac{\partial P}{\partial X} + Pr\frac{(\mu_{nf}/\mu_f)}{(\rho_{nf}/\rho_f)}\left(\frac{\partial^2 V}{\partial X^2} + \frac{\partial^2 V}{\partial Y^2}\right)$$
$$+ \frac{(\rho\beta)_{nf}}{\rho_{nf}\beta_f}Pr Ra\theta, \tag{7}$$

Fig. 2 Comparison of the streamline between the current results with those of [64] and [65] at Ra $= 1.78 \times 105$

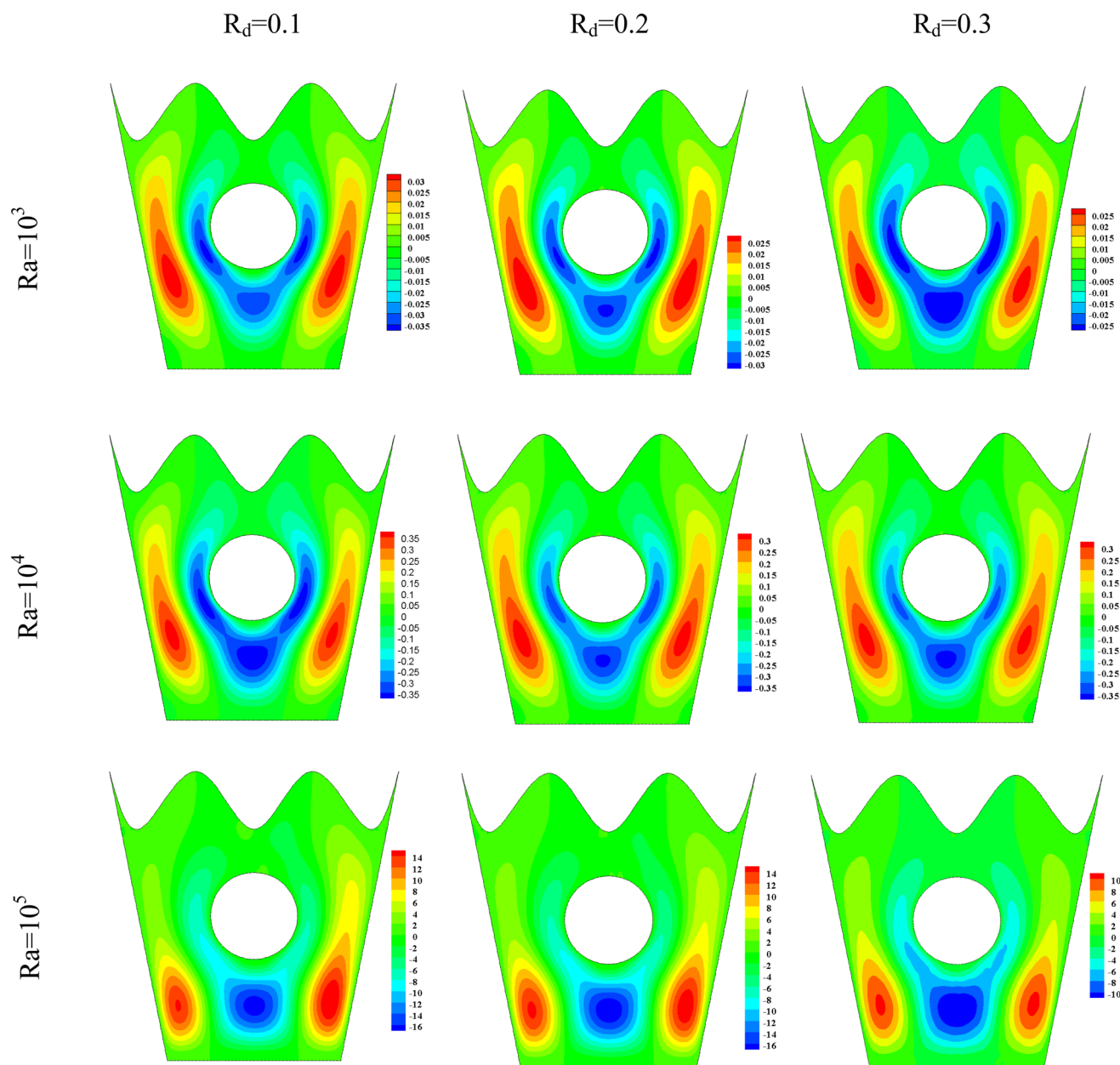**Fig. 3** U-velocity distribution for different Ra and R_d ($\phi = 0.01$)

Eur. Phys. J. Spec. Top. (2022) 231:2713–2731

2717

R_d=0.1   R_d=0.2   R_d=0.3

Ra=10^3

Ra=10^4

Ra=10^5

Fig. 4 V-velocity distribution for different Ra and R_d ($\phi = 0.01$)

$$U\frac{\partial \theta}{\partial X} + V\frac{\partial \theta}{\partial Y} = \frac{(k_{nf}/k_f)}{((\rho C_p)_{nf}/(\rho C_p)_f)}\left(\frac{\partial^2 \theta}{\partial X^2} + \frac{\partial^2 \theta}{\partial Y^2}\right)$$
$$+ \frac{4}{3}\frac{1}{((\rho C_p)_{nf}/(\rho C_p)_f)}Rd\frac{\partial^2 \theta}{\partial Y^2}, \quad (8)$$

where

$$\text{Pr} = \frac{v_f}{\alpha_f}, Ra = g\beta_f(T_h - T_c)\text{L}^3, Rd = \frac{4\sigma_r T_c^3}{\chi_r k_f}. \quad (9)$$
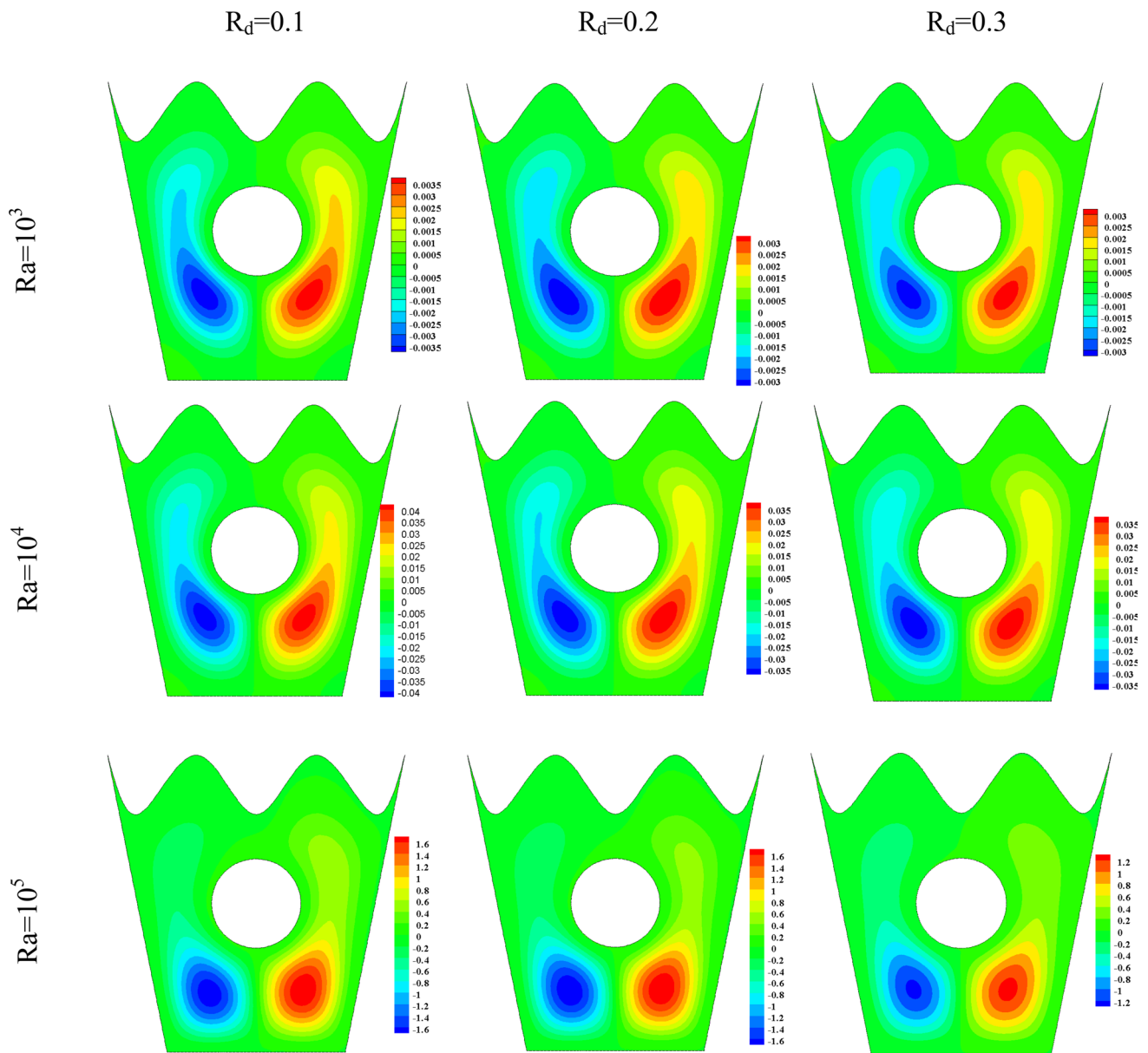
With the boundary conditions:

Left wall: $\frac{\partial \theta}{\partial n} = 0, V = 0\,U = 0$

Right wall: $V = 0, U = 0, \frac{\partial \theta}{\partial n} = 0$

Bottom wall $(Y = 0) : V = 0, U = 0, \frac{\partial \theta}{\partial Y} = -1$

Cylinder and Wavy wall: $\theta = 0, V = 0, U = 0$.
$$(10)$$

The n may be a vector normal to the surfaces of the enclosure at every point. The Nusselt number (local as well as average), on the other hand, would be specified as:

$$\text{Nu} = \left(1 + \frac{4}{3}\frac{k_f}{k_{nf}}\text{Rd}\right)\left(\frac{k_{nf}}{k_f}\right)\left(\frac{1}{\theta}\right), \quad (11)$$

$$\text{Nu}_{\text{avg}} = \frac{1}{2\pi}\int\limits_0^{2\pi}\text{Nu}d\xi. \quad (12)$$

Fig. 5 Streamline distribution for different Ra and R_d ($\phi = 0.01$)

The thermo-physical correlations of TiO$_2$-H$_2$O would be defined as:

$$\rho_{nf} = \phi\rho_s + (1-\phi)\rho_f, \tag{13}$$

$$(\rho C_p)_{nf} = (\rho C_p)_f(1-\phi) + (\rho C_p)_s\phi, \tag{14}$$

$$(\rho\beta)_{nf} = (\rho\beta)_f(1-\phi) + (\rho\beta)_s\phi, \tag{15}$$

$$\alpha_{nf} = \frac{k_{nf}}{(\rho C_p)_{nf}}. \tag{16}$$

The nano-suspension thermal conductivity is defined as:

$$\frac{K_{nf}}{K_f} = \frac{(K_{eq} - 2K_f) - 2(K_{eq} - K_f)(1-\gamma)^3\phi}{(K_{eq} + 2K_f) - (K_{eq} - K_f)(1-\gamma)^3\phi}, \tag{17}$$

where $\gamma = \frac{h_{nl}}{r_p}$, and the equivalent thermal conductivity of the nanoparticles (K$_{eq}$) is:

$$\frac{K_{eq}}{K_s} = \zeta\frac{2(1-\zeta) + (1-\gamma)^3(1+2\zeta)}{-(1-\zeta) + (1-\gamma)^3(1+2\zeta)}, \tag{18}$$

in which $\zeta = \frac{K_{nl}}{K_p}$. For the present study, the assumptions are as follows: $K_{nl} = 100K_f$, $r_p = 3$ nm, and $h_{nl} = 2$ nm [59].

The equations for entropy generation (S) would be [60]:

$$S_{gen} = S_{HT} + S_{FF}, \tag{19}$$

S$_{HT}$ and S$_{FF}$ are the local S in which heat transfer and fluid friction are, respectively, responsible and are expressed as:
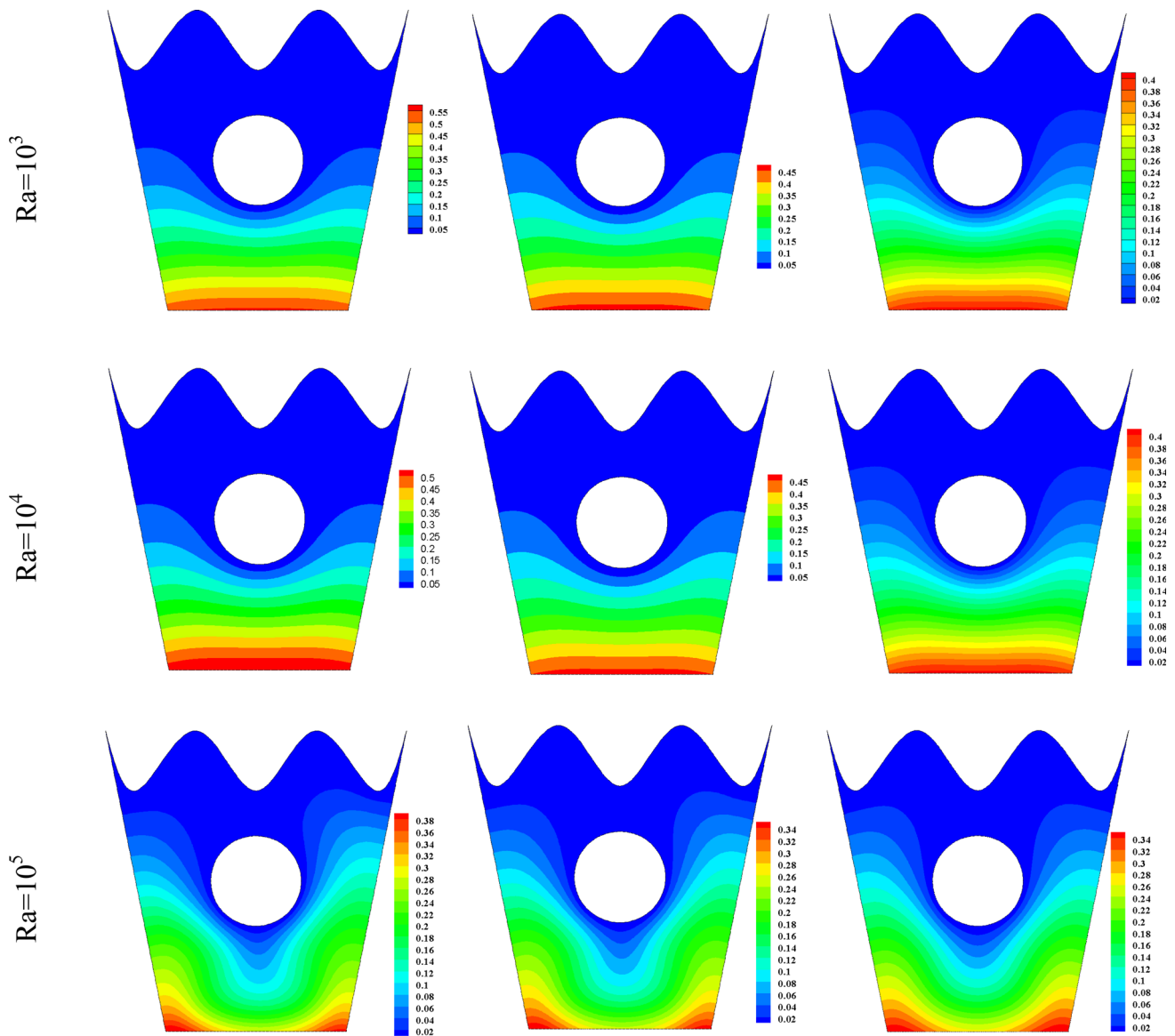
Fig. 6 Isotherm distribution for different Ra and R_d ($\phi = 0.01$)

$$S_{\mathrm{HT}} = \frac{k_{nf}}{k_f} \left[\left(\frac{\partial \theta}{\partial X} \right)^2 + \left(\frac{\partial \theta}{\partial Y} \right)^2 \right], \quad (20)$$

$$S_{FF} = \phi_n \frac{\mu_{nf}}{\mu_f} \left(2 \left(\left(\frac{\partial V}{\partial Y} \right)^2 + \left(\frac{\partial U}{\partial X} \right)^2 \right) \right.$$

$$\left. + \left(\frac{\partial U}{\partial Y} + \frac{\partial V}{\partial X} \right)^2 \right). \quad (21)$$

The Bejan number is:

$$\mathrm{Be} = \frac{S_{\mathrm{HT}}}{S_{\mathrm{gen}}}. \quad (22)$$

3 Validation and numerical analysis

A Finite element method (FEM) is used to solve the conservation equations [20]. This method is in terms of Galerkin method and divides the domain into subdomains and then combines the elements again. The conditions in a two-way coordinate in the FEM method in a specific point are related to the upstream and downstream of that point. Based on the mentioned points, the Flex-PDE software is used to solve the governing equations. This software solves the continuity, momentum, and energy equations with the defined boundary conditions by Galerkin finite element method (GFEM). For solving momentum and continuity, the P_2-P_1 Lagrange finite element is used, and for energy equation, the Lagrange-quadratic finite element is considered [61]. Besides, the convergence criterion for this solution is when the error of the residuals is less than

2720

Eur. Phys. J. Spec. Top. (2022) 231:2713–2731

<div align="center">R_d=0.1   R_d=0.2   R_d=0.3</div>
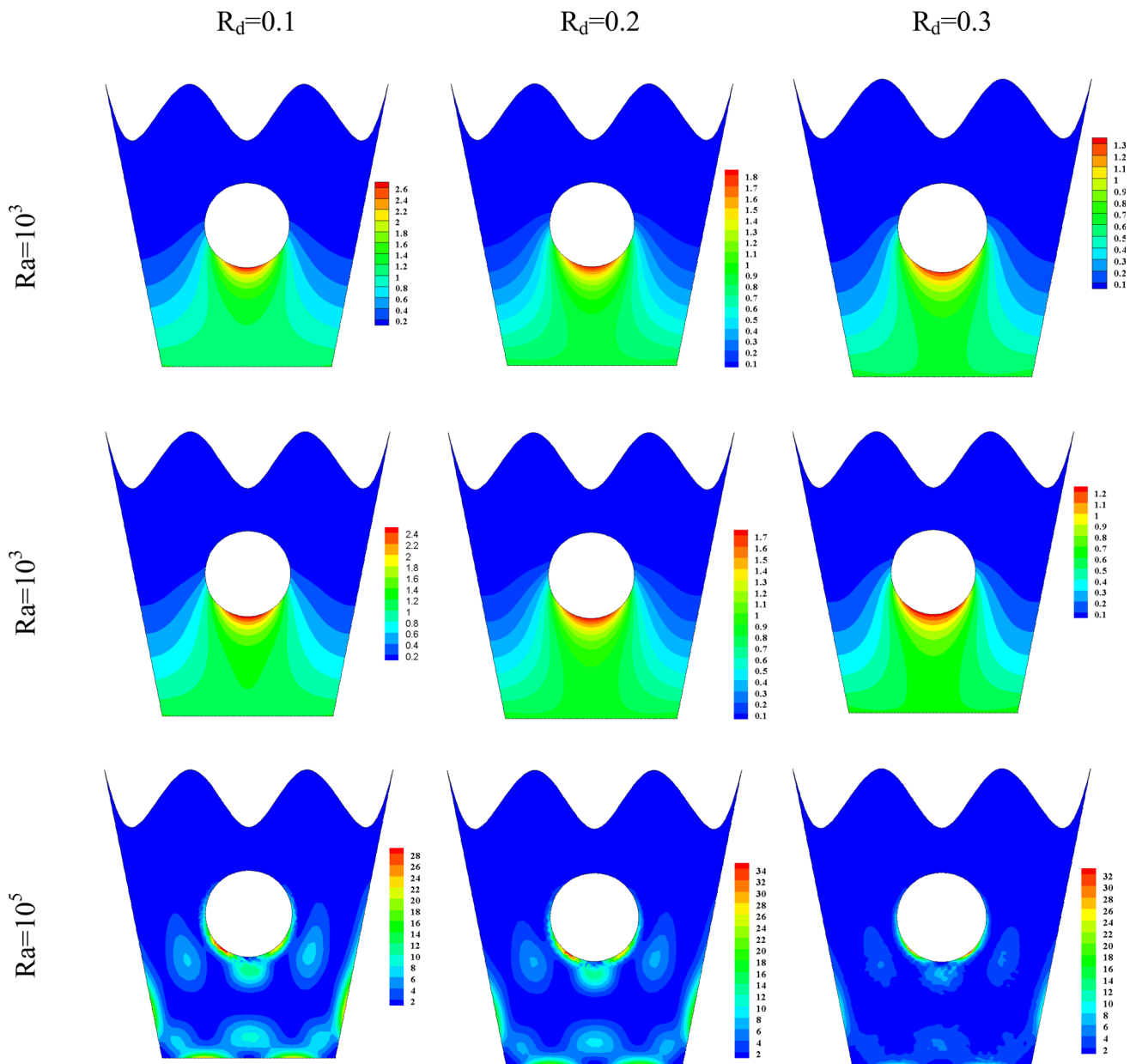
Fig. 7 Local entropy generation for different Ra and R_d ($\phi = 0.01$)

10^{-5}. The following solutions for velocities (U, V) and temperature (θ) are introduced based on Galerkin finite element method [62,63]:

$$U \cong \sum_{n=1}^{N} U_n \gamma_n(X,Y), V \cong \sum_{n=1}^{N} V_n \gamma_n(X,Y),$$

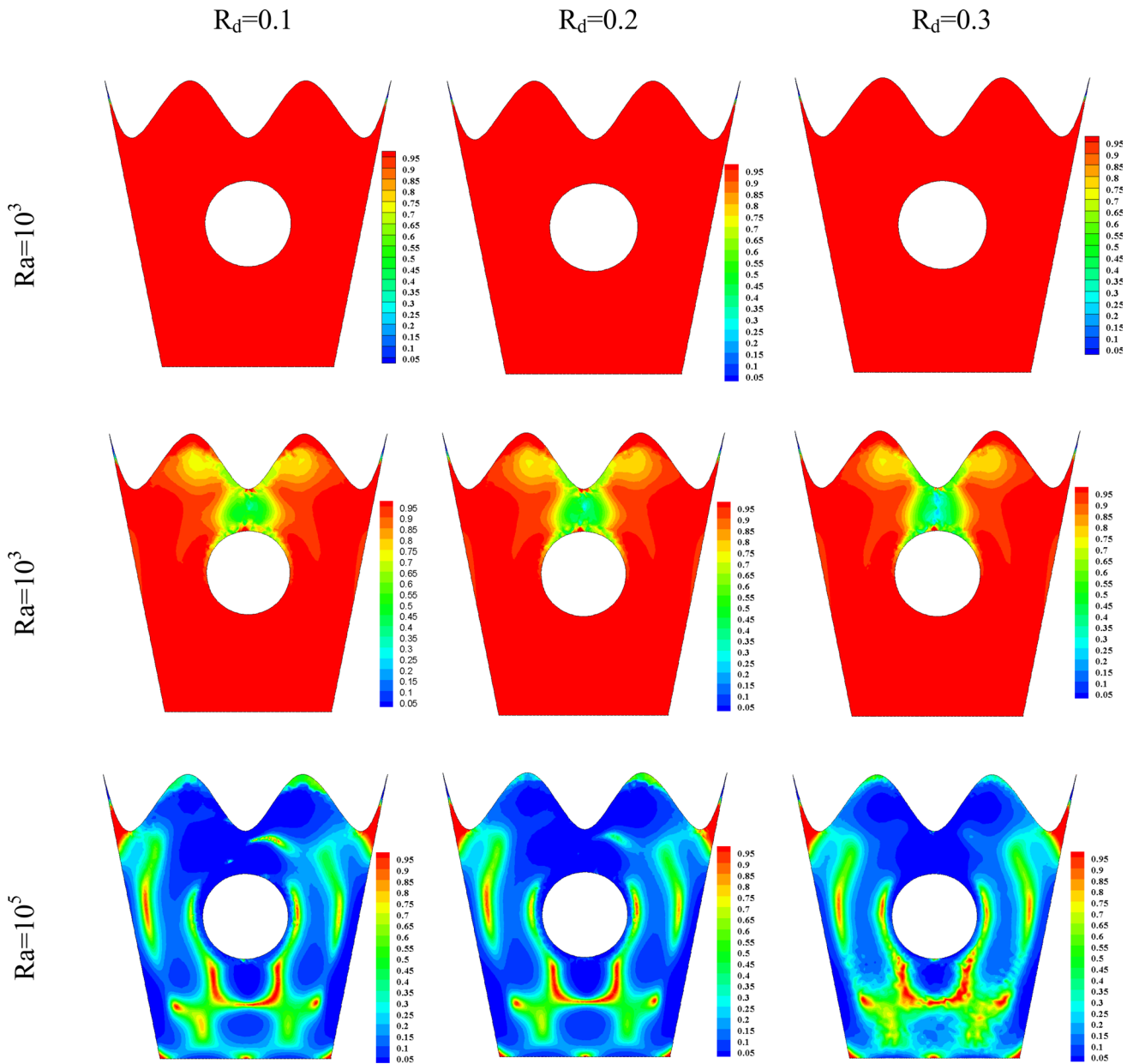$$\theta \cong \sum_{n=1}^{N} \theta_n \gamma_n(X,Y). \tag{23}$$

If one incorporates these equations to 6–8, then the nonlinear residual equations at all nodes of the internal domain on the trash bin cavity will be:

$$R_K^U = \sum_{n=1}^{N} U_n \int_{\Omega} \left[\left(\sum_{n=1}^{N} U_n \gamma_n \right) \frac{\partial \gamma_n}{\partial X} \right.$$

$$+ \left(\sum_{n=1}^{N} V_n \gamma_n \right) \frac{\partial \gamma_n}{\partial Y} \right] \gamma_k dX dY$$

$$+ \Upsilon \left[\sum_{n=1}^{N} U_n \int_{\Omega} \frac{\partial \gamma_k}{\partial X} \frac{\partial \gamma_n}{\partial X} dX dY \right.$$

$$+ \sum_{n=1}^{N} V_n \int_{\Omega} \frac{\partial \gamma_k}{\partial X} \frac{\partial \gamma_n}{\partial Y} dX dY \right]$$

$$+ \Pr \sum_{n=1}^{N} U_n \int_{\Omega} \left[\frac{\partial \gamma_k}{\partial X} \frac{\partial \gamma_n}{\partial X} + \frac{\partial \gamma_k}{\partial Y} \frac{\partial \gamma_n}{\partial Y} \right] dX dY, \tag{24}$$

$$R_K^V = \sum_{n=1}^{N} U_n \int_{\Omega} \left[\left(\sum_{n=1}^{N} U_n \gamma_n \right) \frac{\partial \gamma_n}{\partial X} \right.$$
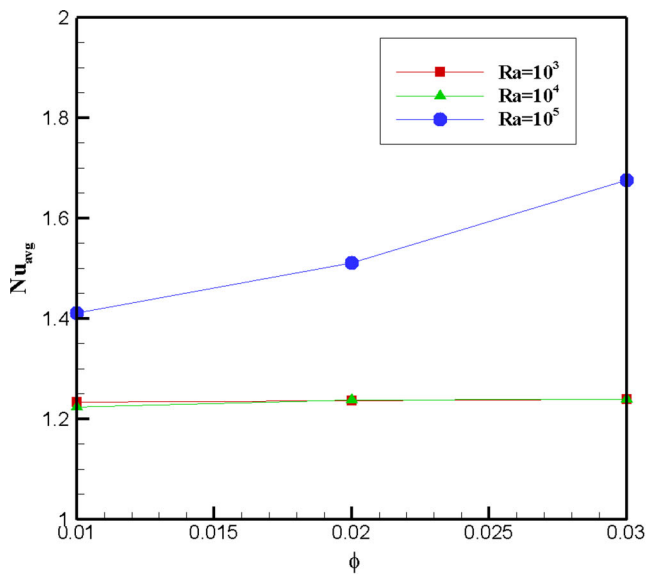
Fig. 8 Bejan number distribution for different Ra and R$_\text{d}$ ($\phi = 0.01$)
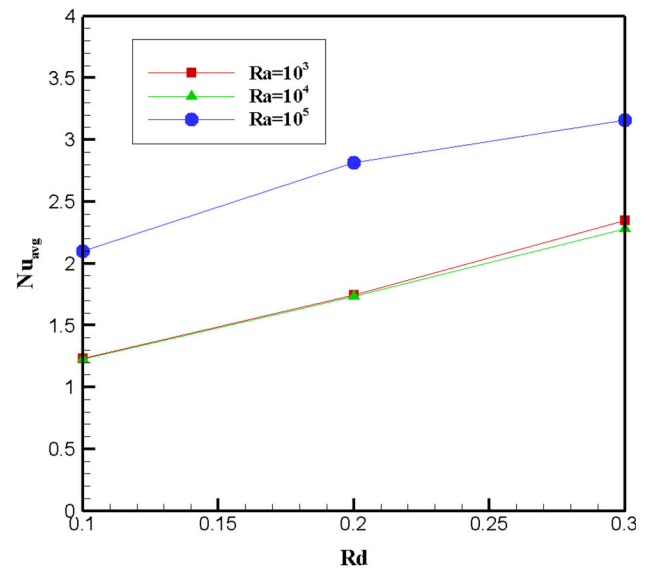
$$+\left(\sum_{n=1}^{N} V_n\gamma_n\right)\frac{\partial\gamma_n}{\partial Y}\Bigg]\gamma_k dXdY$$

$$+\Upsilon\left[\sum_{n=1}^{N} U_n\int_\Omega \frac{\partial\gamma_k}{\partial X}\frac{\partial\gamma_n}{\partial X}dXdY\right.$$

$$+\sum_{n=1}^{N} V_n\int_\Omega \frac{\partial\gamma_k}{\partial X}\frac{\partial\gamma_n}{\partial Y}dXdY\Bigg]$$

$$+\Pr\sum_{n=1}^{N} U_n\int_\Omega\left[\frac{\partial\gamma_k}{\partial X}\frac{\partial\gamma_n}{\partial X}+\frac{\partial\gamma_k}{\partial Y}\frac{\partial\gamma_n}{\partial Y}\right]dXdY$$

$$-\Pr Ra\left(\sum_{n=1}^{N}\theta_n\int_\Omega \gamma_n\gamma_k dXdY\right), \tag{25}$$

$$R_K^\theta = \sum_{n=1}^{N}\theta_n\int_\Omega\left[\left(\sum_{n=1}^{N} U_n\gamma_n\right)\frac{\partial\gamma_n}{\partial X}\right.$$

$$+\left(\sum_{n=1}^{N} V_n\gamma_n\right)\frac{\partial\gamma_n}{\partial Y}\Bigg]\gamma_k dXdY$$

$$+\left(1+\frac{4}{3}\text{Rd}\right)\sum_{n=1}^{N}\theta_n\int_\Omega\left[\frac{\partial\gamma_k}{\partial X}\frac{\partial\gamma_n}{\partial X}+\frac{\partial\gamma_k}{\partial Y}\frac{\partial\gamma_n}{\partial Y}\right]dXdY$$

$$-\lambda\left(\sum_{n=1}^{N}\theta_n\int_\Omega \gamma_n\gamma_k dXdY\right). \tag{26}$$

The case with no fins has the best isotherm distribution among the other cases (Fig. 11). The range of

2722

Eur. Phys. J. Spec. Top. (2022) 231:2713–2731

(a) the effect of nanoparticle concentration on

Nu_{avg} (Rd=0.1)

(b) the effect of radiation parameter on Nu_{avg}

(ϕ=0.01)

Fig. 9 **a** The effect of nanoparticle concentration on Nu_{avg} (Rd = 0.1). **b** The effect of radiation parameter on Nu_{avg} (ϕ = 0.01)

temperature change is minimum for this case and when $Ra = 10^5$.

The Eqs. (24–26) are scrutinized by the reduced integration method and Newton Raphson approach. Then, the 4N*4N system of equations at each iteration will be:

$$J(a^n) \left[a^n - a^{n+1}\right] = R(a^n), \qquad (27)$$

where the Jacobian matrix is $J(a^n)$, and $R(a^n)$ is the residual vector.

Moreover, the results of [64] and also [65] are used to validate the present code. The results show that there is a negligible difference between these analyses and the code is valid.

Moreover, to validate the results of the present work with the wavy wall geometries studied before, the results are compared with those of Oztop et al. [66] in Table 2. Again, the results are in good agreement with Ref. [66].

4 Results

4.1 Geometry with no fin

The outcomes of the present study are introduced and analyzed in two plans: first of all, the thermal parameters' impact on the Nu and S is studied when there is no fin attached to the middle circle. Figure 3 shows the contours of U-velocity for varying Rd and Ra. There

may be four counter-rotating cells that exist owing to density diversity. These cells will be more potent if Ra goes up from 10^3 to 10^5. Besides, the maximum value of U-velocity goes up from 0.03 to 12 if Ra increases. On the other hand, the radiation has a negative impact on the maximum amount of U-velocity. V-velocity has also the same attitude toward changes in Ra and Rd. Figure 4 depicts the contours of V-velocity. One is able to see that Ra has a positive and Rd has a reverse impact on this parameter. This is because higher Ra means better buoyancy-driven flow and better movement of nanofluid. However, Higher Rd means more contribution of conduction heat transfer to thermal radiation. Based on Figs. 3 and 4, one can conclude that the radiation parameter can be used as a tool to control the power of fluid flow within the thermal systems.

The distribution of streamlines is depicted in Fig. 5. There are two main and big counter-rotating cells with high intensity around the circle. The main reason is the difference between the density of the hot flow coming from the bottom wall and the cold wall of the circle. For the cases in which the intensity of the streamline is important such as pipes and the force of the fluid flow on them, this behavior is of interest. Moreover, the highest amount of streamline happens when $Ra = 10^5$ and $Rd = 0.1$.

The isotherm distribution which is responsible for temperature distribution inside the cavity is shown in Fig. 6. The isotherms are distributed uniformly due to constant heat flux of the bottom wall. The lower sections of the cavity have higher amount of isotherms and by coming up to the wavy wall this amount reduces.
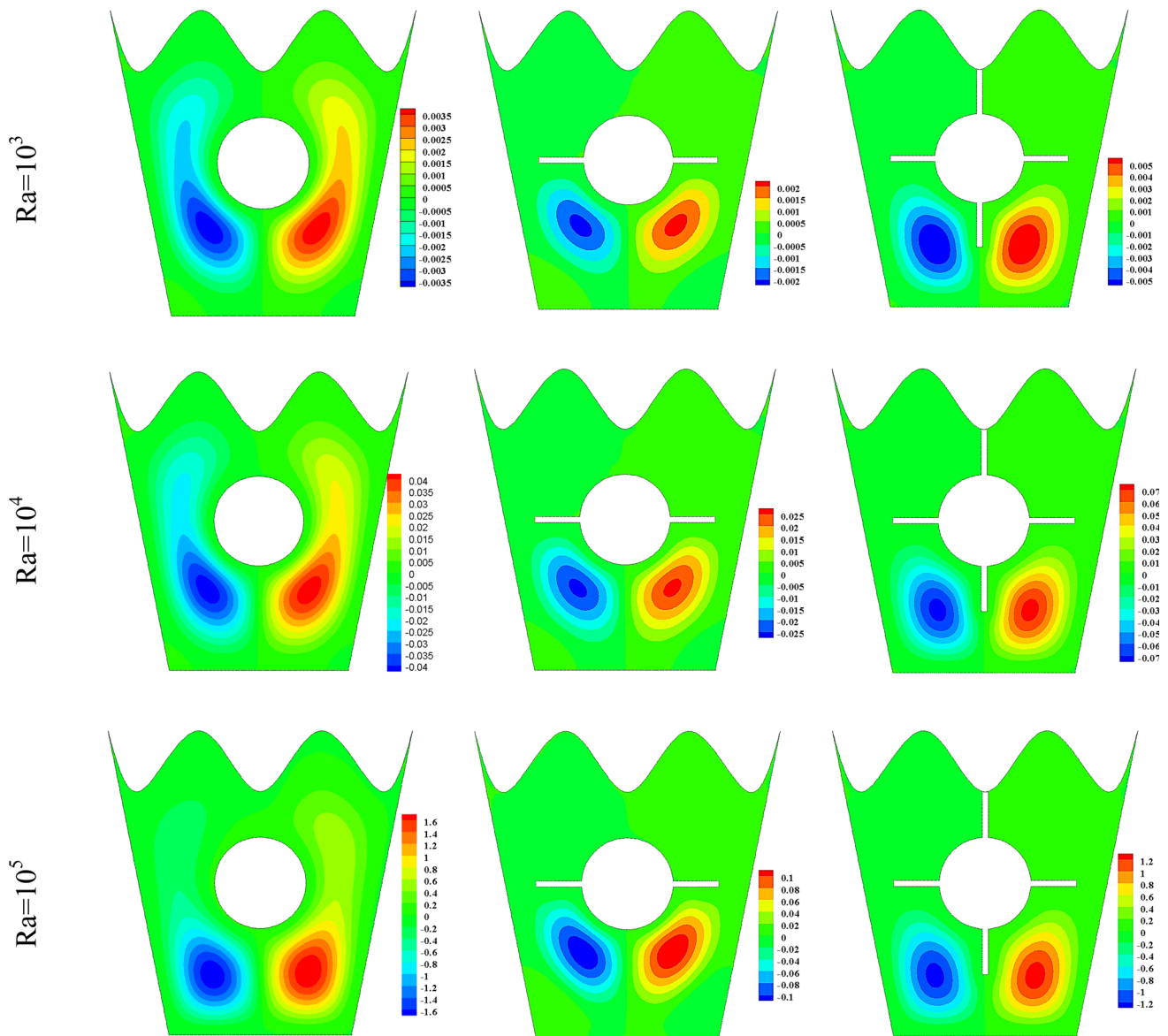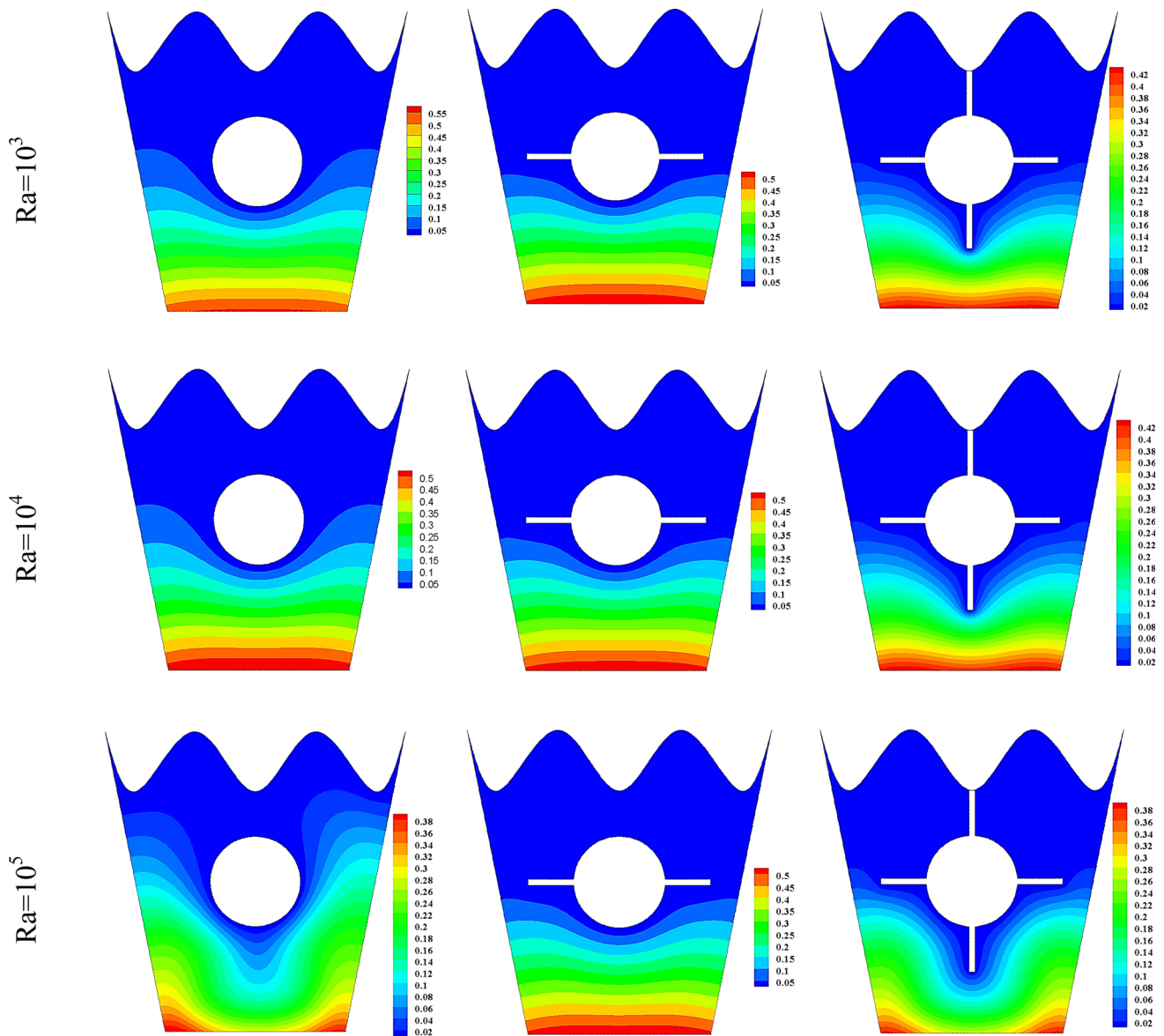
Fig. 10 Streamline distribution for variable numbers of fins ($\phi = 0.01$, $Rd = 0.1$)

The maximum amount of isotherm is seen for the case with $Ra = 10^3$ and $Rd = 0.1$. However, the distribution of isotherms is smoother for the case with $Ra = 10^5$ and $Rd = 0.3$.

Local S and Bejan number are other interesting parameters in this study. The entropy generation here is due to heat transfer and friction between the base fluid and nanoparticles. This factor increases by going up the Rayleigh number (Fig. 7). Furthermore, the maximum value of local S takes place at the lower section of the circle. This is the place where the hot and cold flows are intertwined to each other rigorously which means there is more loss of energy at this point. Increasing the Rayleigh number is responsible for a decrease in Bejan number (Fig. 8). Bejan number is defined as the ratio of irreversibility due to heat transfer to the total irreversibility. When the Ra increases, the buoyancy-driven flow is enhanced and the natural convection heat

transfer also becomes better. This means lower irreversibility in heat transfer and accordingly lower Bejan number. Radiation has a very slight positive impact on Bejan number, especially for the case ($Ra = 10^5$). The increase in Be due to increasing radiation parameter clearly shows that Rd has a negative impact on the stability of energy systems.

Nanoparticle concentration and radiation parameter are the two factors which affect the Nu_{avg}. Figure 9a shows that increasing ϕ enhances the average Nusselt number for the case $Ra = 10^5$. This increase is 19%. For the two other cases, there is no change in Nu_{avg}. On the other hand, the radiation parameter enhances Nu_{avg} for all the cases of Ra (Fig. 9b). This behavior shows that Rd is a positive factor as one of the procedures for heat transfer enhancement.

Fig. 11 Isotherm distribution for variable number of fins ($\phi = 0.01$, Rd $= 0.1$)

4.2 The geometry with fin

In the second plan, the geometry's impact on heat transfer is perused. The number of fins, the shape of the fin, and the geometry of wavy wall are the geometrical parameters changed to see the effects on Nu and S. The effect of fin number of streamline distribution reveals that the case with two fins has the minimum intensity of rotating vortices below the cylinder and has the best streamline distribution (Fig. 10). Besides, adding two fins reduces the intensity of maximum streamlines up to 94% due to the fact that the fins block the flow from moving around the cylinder.

The effect of fin number on local S and Bejan number is depicted in Figs. 12 and 13, respectively. S due to fluid friction and heat transfer increases by increasing the number of the fins. For the case with four fins, this increase in very noticeable, which means increas-

ing the fins causes a huge irreversibility of flow in the cavity. Interestingly, the best distribution of the Bejan number is for the case with four fins. This means that the irreversibility due to heat transfer is the lowest for the case for four fins (Fig. 13). These two figures reveal that increasing the fin number is the main cause for increasing the friction loss; however, it reduces the irreversibility due to heat transfer.

The effect of fin number on $\mathrm{Nu_{avg}}$ is obtained for different parameters in Table 3. Overall, the fin number has a useful influence on $\mathrm{Nu_{avg}}$. This means that increasing the number of fins enhances the overall NC heat transfer of the bottom wall. The maximum increase in $\mathrm{Nu_{avg}}$ is obtained for the case with Ra $= 10^4$. Accordingly, if one wants to enhance heat transfer in industrial applications, increasing the number of the fins is one solution. Furthermore, $\mathrm{Nu_{avg}}$ will be enhanced by 30% for the case with Ra $= 10^3$, 29%

No fin   Two fins   Four fins

Ra=10^3
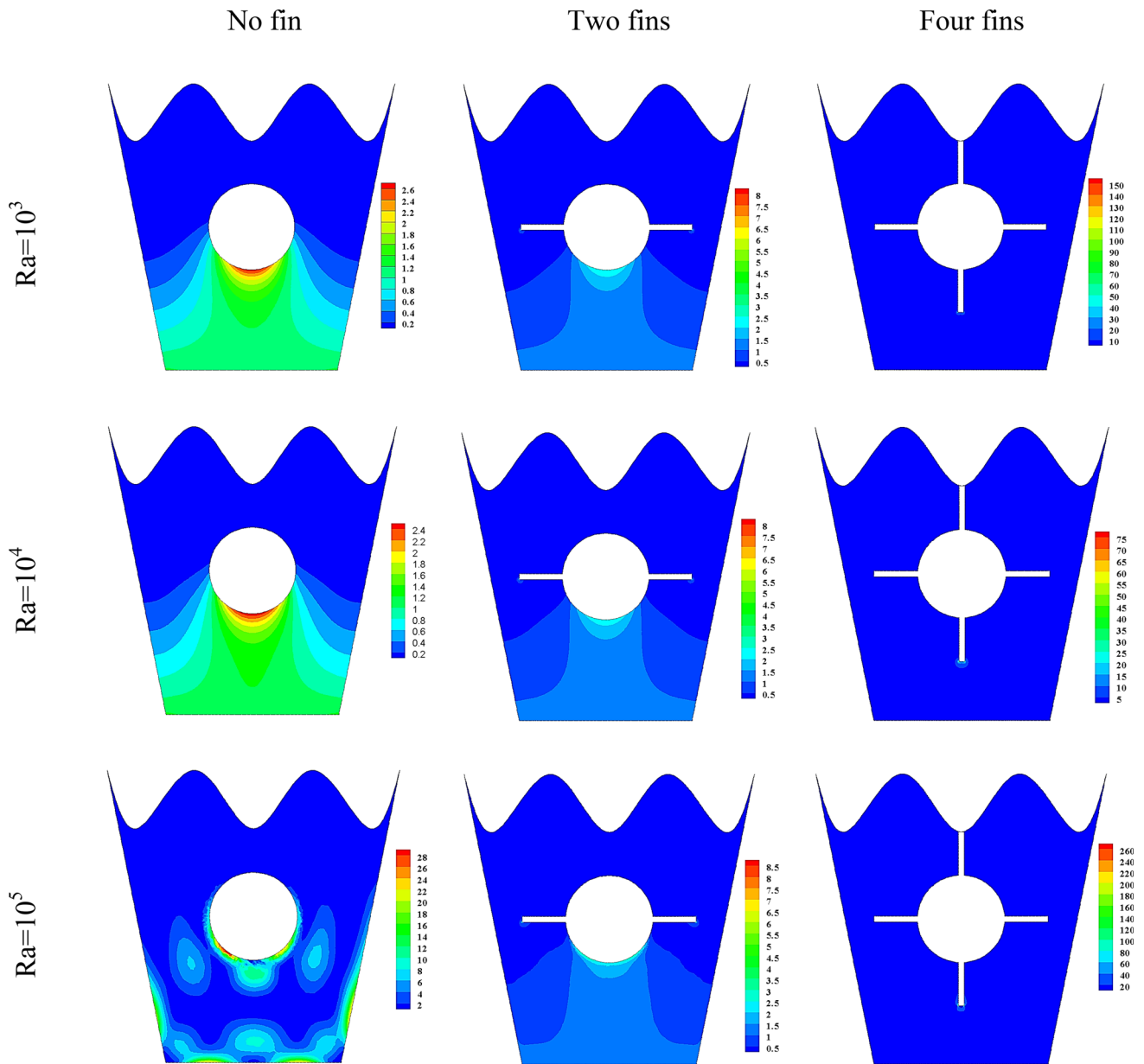
Ra=10^4

Ra=10^5

Fig. 12 Local entropy distribution for different number of fins ($\phi = 0.01$, Rd = 0.1)

for the case with Ra = 10^4, and 54% for the case with Ra = 10^5, when the number of fins increases from zero to four. So, it can be concluded that the effect of fin's number is superior for the case with Ra = 10^5.

The effect of fin size is also studied in this research. Three different fin sizes are considered (L = r, L = r/2, L = r/4), in which r is the radius of the circle. The intensity of the cells increases by increasing the length of the fin; however, the area of the cells reduces (Fig. 14a). Besides, the isotherms are more uniform for the last case with the largest fin size (Fig. 14b), and the Bejan number reduces at the upper side of the cavity for the case with L = r (Fig. 14c).

The effect of wavy wall is studied in Fig. 15. Three shapes of wavy wall with different amplitudes (0.05, 0.075, and 0.1) and fixed undulation (2) are considered.

The average fin size (L = r/2) is used for this simulation. The intensity of vortices is reduced by increasing the amplitude. Besides, the Bejan number increases by increasing the amplitude from 0.05 to 0.1. Moreover, Table 4 shows the amount of $\mathrm{Nu_{avg}}$ for these three cases. The amplitude of wavy wall has a reverse influence on $\mathrm{Nu_{avg}}$. The $\mathrm{Nu_{avg}}$ lessens by 22% when the amplitude is increased from 0.05 to 0.075.

5 Conclusion

Natural convection (NC) and entropy generation (S) of the TiO$_2$-H$_2$O nanofluid is studied in a trash bin-shaped wavy wall cavity. Two scenarios are considered:

| No fin | Two fins | Four fins |
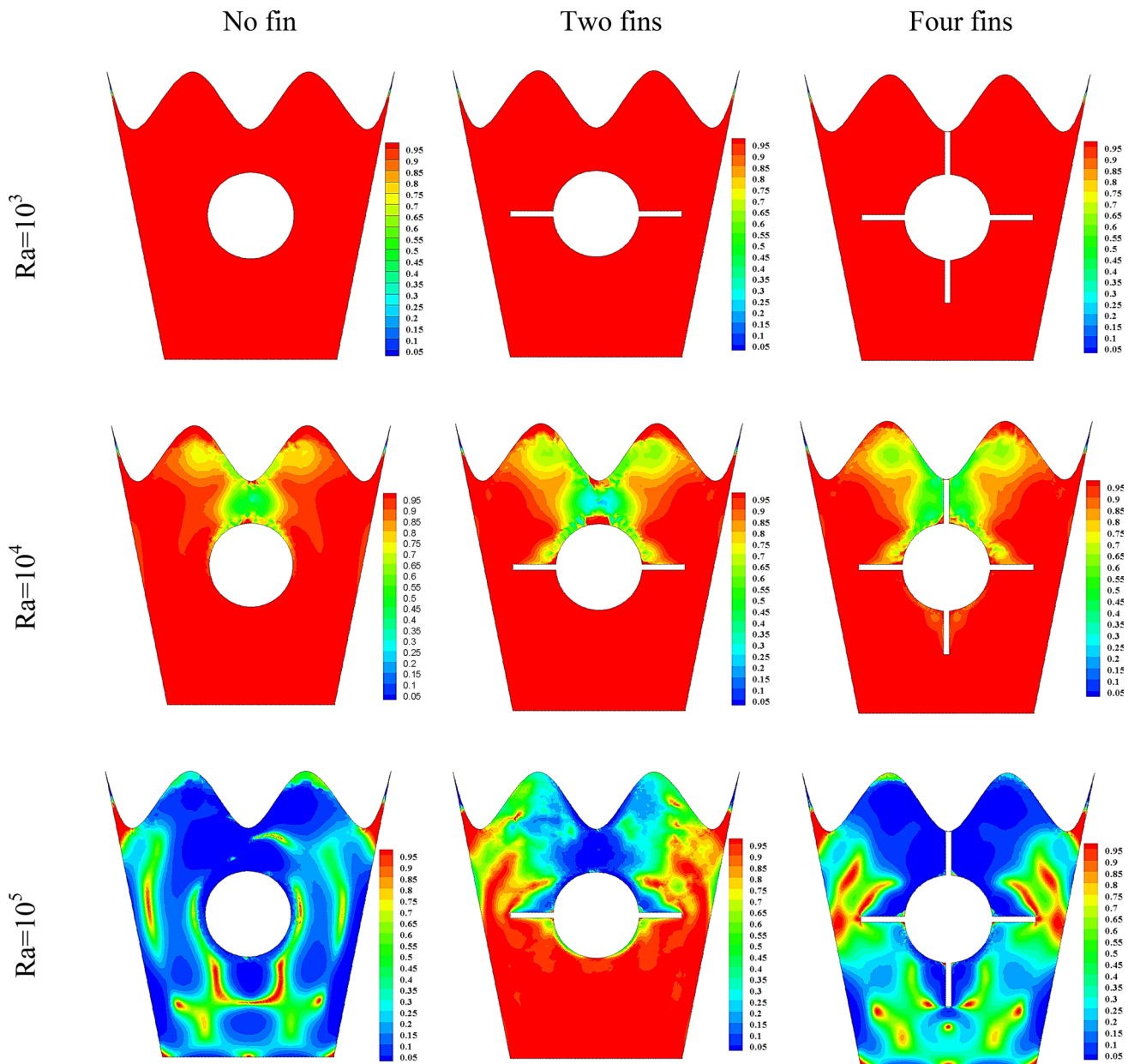
Fig. 13 Bejan number for different number of fins ($\phi = 0.01$, Rd = 0.1)

Table 3 The effect of fin number on Nu$_{avg}$

	ϕ	Rd	Number of fin	Nu$_{avg}$
Ra = 10^3	0.01	0.1	0	1.2231
	0.01	0.1	2	1.2442
	0.01	0.1	4	1.5931
Ra = 10^4	0.01	0.1	0	1.2338
	0.01	0.1	2	1.2558
	0.01	0.1	4	1.5970
Ra = 10^5	0.01	0.1	0	1.4103
	0.01	0.1	2	1.5342
	0.01	0.1	4	2.1667
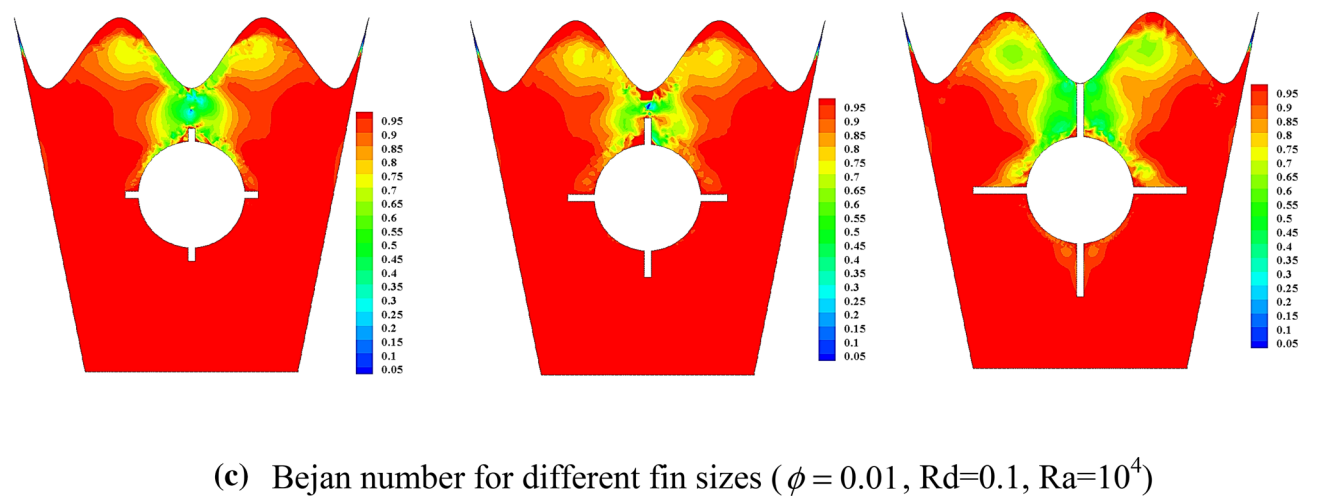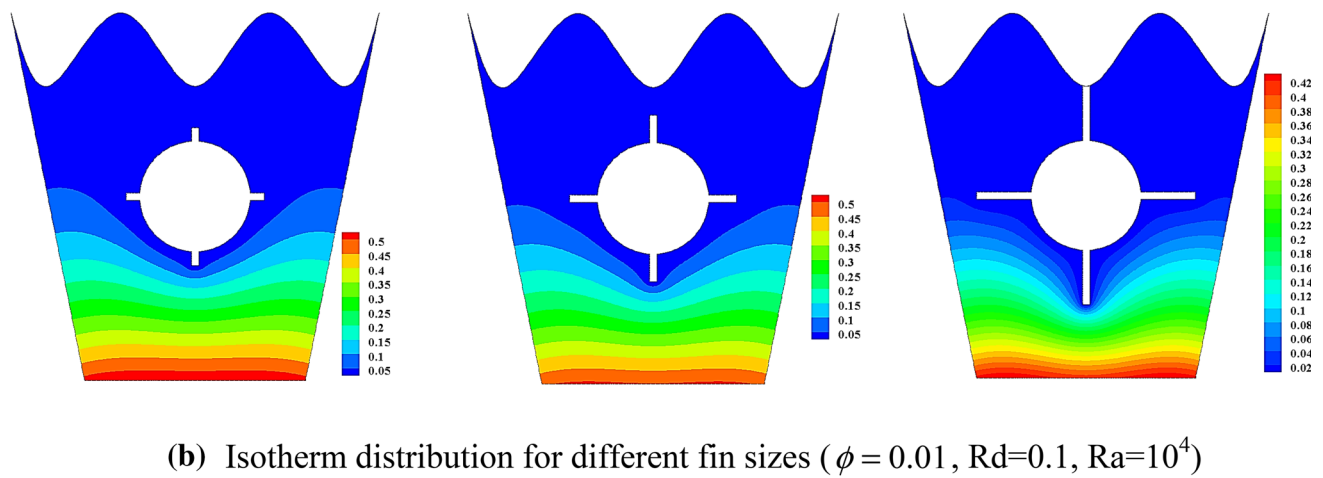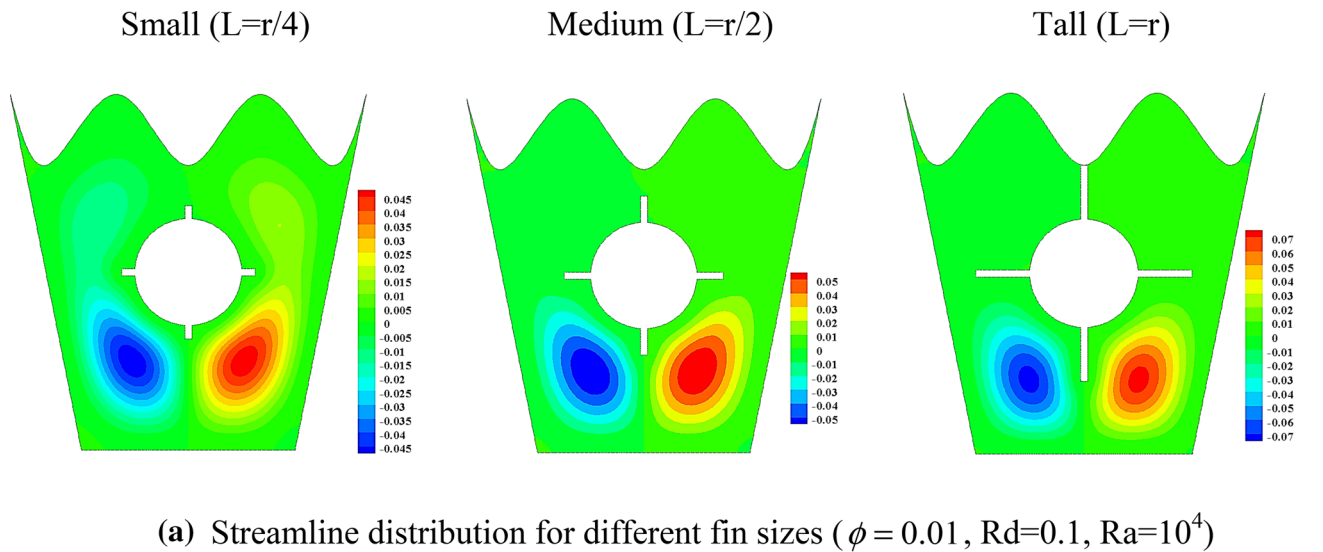
(a) Streamline distribution for different fin sizes ($\phi = 0.01$, Rd=0.1, Ra=10^4)

(b) Isotherm distribution for different fin sizes ($\phi = 0.01$, Rd=0.1, Ra=10^4)

(c) Bejan number for different fin sizes ($\phi = 0.01$, Rd=0.1, Ra=10^4)

Fig. 14 **a** Streamline distribution for different fin sizes ($\phi = 0.01$, Rd = 0.1, Ra = 104). **b** Isotherm distribution for different fin sizes ($\phi = 0.01$, Rd = 0.1, Ra = 104). **c** Bejan number for different fin sizes ($\phi = 0.01$, Rd = 0.1, Ra = 10^4)

Small wavy wall   Medium wavy wall   Large wavy wall

(**a**) Streamline distribution for different wavy sizes ($\phi = 0.03$, Rd=0.1, Ra=10^5)

(**b**) Isotherm distribution for different wavy sizes ($\phi = 0.03$, Rd=0.1, Ra=10^5)

(**c**) Bejan number for different wavy sizes ($\phi = 0.03$, Rd=0.1, Ra=10^5)

Fig. 15 **a** Streamline distribution for different wavy sizes ($\phi = 0.03$, Rd = 0.1, Ra = 105). **b** Isotherm distribution for different wavy sizes ($\phi = 0.03$, Rd = 0.1, Ra = 105). **c** Bejan number for different wavy sizes ($\phi = 0.03$, Rd = 0.1, Ra = 10^5)

Eur. Phys. J. Spec. Top. (2022) 231:2713–2731

2729
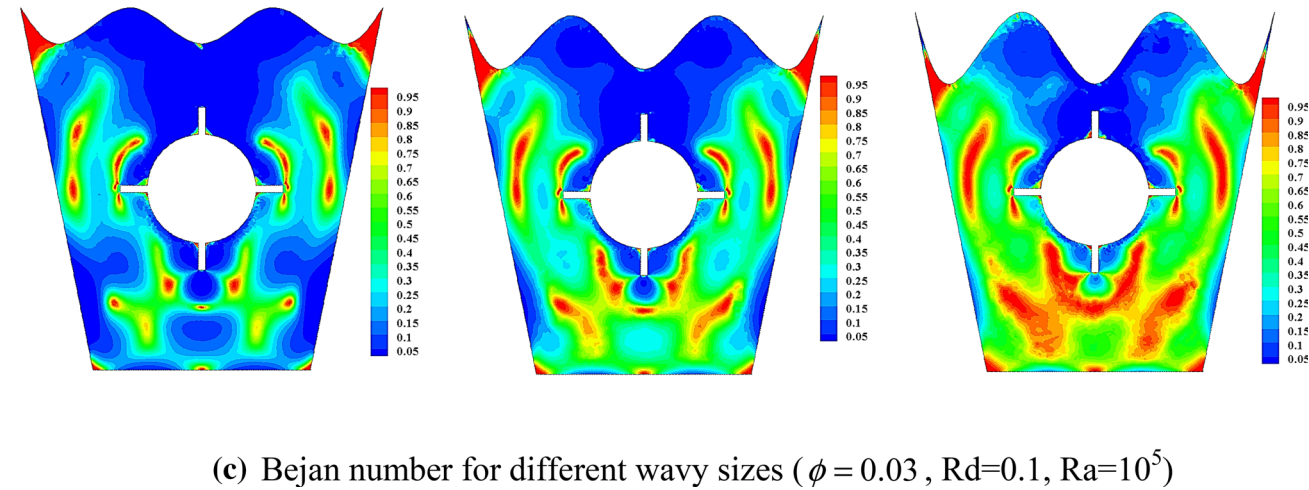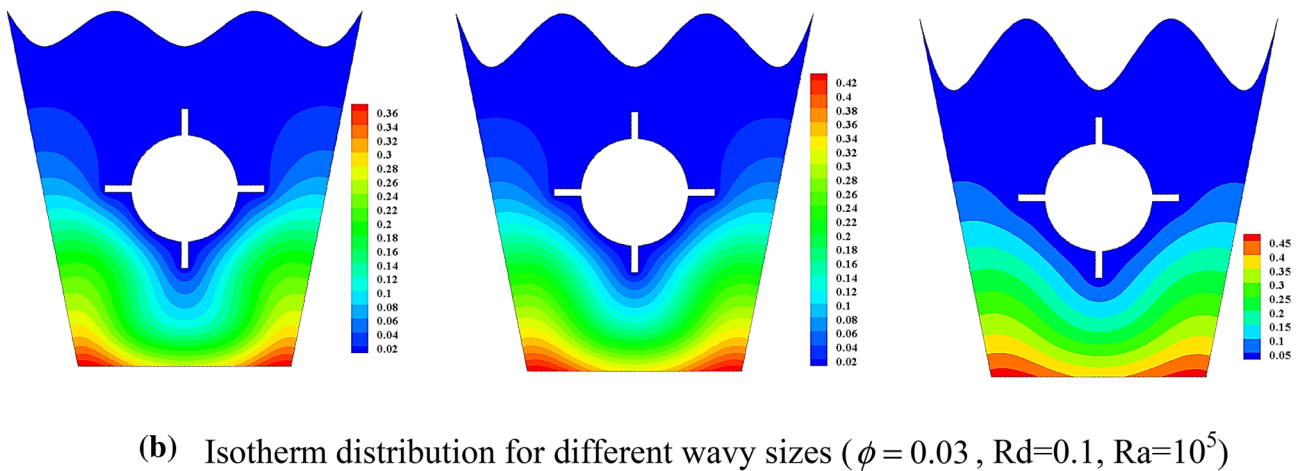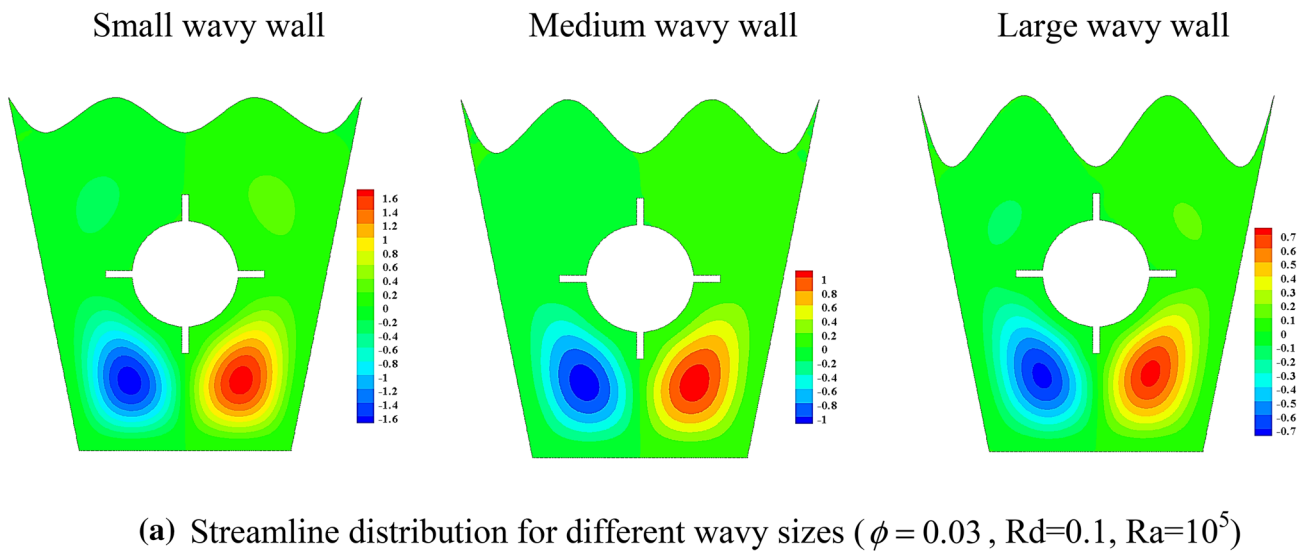
Table 4 The wavy wall amplitude's impact on Nu_{avg} ($\phi = 0.03$, $Rd = 0.1$, $Ra = 10^5$)

Wavy wall amplitude	0.05	0.075	0.1
Nu_{avg}	1.8090	1.4113	1.2488

in the first scenario, the effects of thermal parameters on the enclosure with bare cylinder inside are examined. In the second plan, the geometry of the wavy wall (amplitude of wavy wall) and fins of the cylinder's impact on NC and S are considered. Some of the most important findings are:

- Increasing Ra causes an increase in streamlines and velocity and decrease in Bejan number.
- Changes in Rd (from 0.1 to 0.3) enhances Nu_{avg} up to 90%.
- Increasing the number of the fins is responsible for reducing the heat transfer irreversibility and increasing the friction irreversibility.
- Increasing the fin number from 0 to 4 enhances the Nu_{avg} by 29%, 31%, and 54% for the cases with $Ra = 10^3$, $Ra = 10^4$, and $Ra = 10^5$, respectively.
- Increasing the length of the fin reduces the irreversibility due to heat transfer. On the other hand, it increases the irreversibility due to friction.
- The best Nu_{avg} is obtained for the wavy wall with the least amplitude (0.05), and if the amplitude is increased from 0.05 to 0.1, the Nu_{avg} reduces by 31%.
- The Bejan number increases by increasing the amplitude of the wavy wall.

References

1. S.U.S Choi, J. Eastman, Enhancing thermal conductivity of fluids with nanoparticles. ASME Int. Mech. Eng. Congress Expos. **66**, 99–105 (1995)
2. B. Durand-Estebe, C. Le Bot, E. Arquis, Validation of turbulent natural convection in a square cavity for application of CFD modeling to heat transfer and fluid flow in a data center. In *Proceedings of the ASME 2012 11th Biennial Conference on Engineering Systems Design and Analysis*, July 2–4, 2012, Nantes, France (2012)
3. H.A. Richmond, K.G.T. Hollands, Numerical solution of an open cavity, natural convection heat exchanger. J. Heat Transfer **111**(1), 80–85 (1989)
4. B.M. Krishne Gowda, M.S. Rajagopal, Aswatha, K.N. Seetharamu. Heat transfer in a side heated trapezoidal cavity with openings. Eng. Sci. Technol. Int. J. **22**, 153–167 (2018)
5. M.G. Parent, T.H. Van der Meer, K.G.T. Hollands, Natural convection heat exchangers in solar water heating systems: theory and experiment. Sol. Energy **45**, 43–52 (1990)
6. M.M. Sarafraz, I. Zhe Tian, S.K. Tlili, M. Goodarzi, Thermal evaluation of a heat pipe working with n-pentane-acetone and n-pentane-methanol binary mixtures. J. Therm. Anal. Calorim. **139**(4), 2435–2445 (2020)
7. H.R. Goshayeshi, M.R. Safaei, M. Goodarzi, M. Dahari, Particle size and type effects on heat transfer enhancement of Ferro-nanofluids in a pulsating heat pipe. Powder Technol. **301**, 1218–1226 (2016)
8. H.F. Oztop, M.A. Almeshaal, L. Kolsi, M.M. Rashidi, M.E. Ali. Natural convection and irreversibility evaluation in a cubic cavity with partial opening in both top and bottom sides. Entropy **21**(2), 1–16 (2019)
9. D.S. Loenko, A. Shenoy, M.A. Sheremet, Natural convection of non-Newtonian power-law fluid in a square cavity with a heat-generating element. Energies **12**(11), 2149 (2019)
10. H. Salehipour, S. Emadi, S. Tayebikhorami, M.A. Shahmohammadi, A semi-analytical solution for dynamic stability analysis of nanocomposite/fibre-reinforced doubly-curved panels resting on the elastic foundation in thermal environment. Eur. Phys. J. Plus **137**(1), 1–36 (2022)
11. M.A. Shahmohammadi, S.M. Mirfatah, S. Emadi, H. Salehipour, Ö. Civalek, Nonlinear thermo-mechanical static analysis of toroidal shells made of nanocomposite/fiber reinforced composite plies surrounded by elastic medium. Thin-Walled Struct. **170**, 108616 (2022)
12. H.R. Ashorynejad, B. Hoseinpour, Investigation of different nanofluids effect on entropy generation on natural convection in a porous cavity. Eur. J. Mech, B/Fluids **62**, 86–93 (2016)
13. S.C. Saha, Scaling of free convection heat transfer in a triangular cavity for Pr>1. Energy Build **43**(10), 2908–17 (2011)
14. H. Saleh, R. Roslan, I. Hashim, Natural convection heat transfer in a nanofluid filled trapezoidal enclosure. Int. J. Heat Mass Transf. **54**, 194–201 (2011)
15. M. Bahiraei, M. Jamshidmofid, M. Goodarzi, Efficacy of a hybrid nanofluid in a new microchannel heat sink equipped with both secondary channels and ribs. J. Mol. Liq. **273**, 88–98 (2019)
16. Q. Sun, I. Pop, Free convection in a triangle cavity filled with a porous medium saturated with nanofluids with flush mounted heater on the wall. Int. J. Therm. Sci. **50**(11), 2141–2153 (2011)
17. H.R. Ashorynejad, B. Hoseinpour, Investigation of different nanofluids effect on entropy generation on natural convection in a porous cavity. Eur. J. Mech, B/Fluids (2016)
18. S. Eshaghi, F. Izadpanah, A.S. Dogonchi, A.J. Chamkha, M.B.B. Hamida, H. Alhumade, The optimum double diffusive natural convection heat transfer in H-Shaped cavity with a baffle inside and a corrugated wall. Case Stud. Therm. Eng. **28**, 101541 (2021)
19. M.H. Bahmani, G. Sheikhzadeh, M. Zarringhalam, O.A. Akbari, A.A.A.A. Alrashed, G.A.S. Shabani, M. Goodarzi, Investigation of turbulent heat transfer and nanofluid flow in a double pipe heat exchanger. Adv. Powder Technol. **29**(2), 273–282 (2018)
20. M. Hatami, Numerical study of nanofluids natural convection in a rectangular cavity including heated fins. J. Mol. Liq. **233**, 1–8 (2017)

2730

Eur. Phys. J. Spec. Top. (2022) 231:2713–2731

21. S. Abdelkaber, R. Mebrouk, B. Abdellah, B. Khadidja, Natural convection in a Horizontal Wavy Enclosure. J. Appl. Sci. **7**, 334–341 (2007)

22. M.T. Nguyen, M.A. Abdelraheem, S.W. Lee, Effect of a wavy interface on the natural convection of a nanofluid in a cavity with a partially layered porous medium using the ISPH method. Num. Heat Transf. Part A: Appl. **72**(1), 68–88 (2017). https://doi.org/10.1080/10407782.2017.1353385

23. M. Waqas, T. Hayat, A. Alsaedi, A theoretical analysis of SWCNT-MWCNT and H 2 O nanofluids considering Darcy-Forchheimer relation. Appl. Nanosci. **9**(5), 1183–1191 (2019)

24. P.S. Rao, P. Barman, Natural convection in a wavy porous cavity subjected to a partial heat source. Int. Commun. Heat Mass Transf. **120**, 105007 (2021)

25. A.S. Dogonchi, A.J. Chamkha, D.D. Ganji, A numerical investigation of magneto-hydrodynamic natural convection of Cu-water nanofluid in a wavy cavity using CVFEM. J. Therm. Anal. Calorim. **135**(4), 2599–2611 (2019)

26. A.S. Dogonchi, M. Hashemi-Tilehnoee, M. Waqas, S.M. Seyyedi, I.L. Animasaun, D.D. Ganji, The influence of different shapes of nanoparticle on Cu-H$_2$O nanofluids in a partially heated irregular wavy enclosure. Physica A **540**, 123034 (2020)

27. S.M. Seyyedi, A.S. Dogonchi, M. Hashemi-Tilehnoee, Z. Asghar, M. Waqas, D.D. Ganji, A computational framework for natural convective hydromagnetic flow via inclined cavity: an analysis subjected to entropy generation. J. Mol. Liq. **287**, 110863 (2019)

28. M. Waqas, S. Jabeen, T. Hayat, S.A. Shehzad, A. Alsaedi, Numerical simulation for nonlinear radiated Eyring-Powell nanofluid considering magnetic dipole and activation energy. Int. Commun. Heat Mass Transfer **112**, 104401 (2020)

29. S.M. Seyyedi, A.S. Dogonchi, M. Hashemi-Tilehnoee, M. Waqas, D.D. Ganji, Investigation of entropy generation in a square inclined cavity using control volume finite element method with aided quadratic Lagrange interpolation functions. Int. Commun. Heat Mass Transfer **110**, 104398 (2020)

30. M. Waqas, A study on magneto-hydrodynamic non-Newtonian thermally radiative fluid considering mixed convection impact towards convective stratified surface. Int. Commun. Heat Mass Transfer **126**, 105262 (2021)

31. M. Waqas, Z. Asghar, W. A. Khan, Thermo-solutal Robin conditions significance in thermally radiative nanofluid under stratification and magnetohydrodynamics. Eur. Phys. J. Special Topics **230**, 1307–1316 (2021)

32. M. Waqas, Simulation of revised nanofluid model in the stagnation region of cross fluid by expanding-contracting cylinder. Int. J. Num. Methods Heat Fluid Flow **29**(4), 2193–2205 (2019)

33. A.M. Aly, Z.A.S. Raizah, S.E. Ahmed, ISPH simulations of natural convection from rotating circular cylinders inside a horizontal wavy cavity filled with a nanofluid and saturated by a heterogeneous porous medium. Eur. Phys. J. Special Topics **230**, 1173–1183 (2021)

34. S.P. Samrat, M. Girinath Reddy, N. Sandeep, Buoyancy effect on magnetohydrodynamic radiative flow of Casson fluid with Brownian moment and thermophoresis. Eur. Phys. J. Special Topics **230**, 1273–1281 (2021)

35. S.E. Ahmed, Z.A.S. Raizah, A.M. Aly, Three-dimensional flow of a power-law nanofluid within a cubic domain filled with a heat-generating and 3D-heterogeneous porous medium. Eur. Phys. J. Special Topics **230**, 1185–1199 (2021)

36. S. Feng, M. Shi, H. Yan, S. Sun, F. Li, L. Tian Jian, Natural convection in a cross-fin heat sink. Appl. Therm. Eng. **132**, 30–37 (2018)

37. H. Saleh, I. Hashim, E. Jamesahar, M. Ghalambaz, Effects of flexible fin on natural convection in enclosure partially-filled with porous medium. Alexandria Eng. J. **59**, 3515–3529 (2020)

38. M. Fayz-Al-Asad, M.J.H. Munshi, M.M.A. Sarker, Effect of fin length and location on natural convection heat transfer in a wavy cavity. Int. J. Thermo-fluid Sci. Technol. **7**(3), 070303 (2020)

39. Y. Khetib, A.A. Alahmadi, A. Alzaed, H. Azimy, M. Sharifpur, G. Cheraghian, Effect of straight, inclined and curved fins on natural convection and entropy generation of a nanofluid in a square cavity influenced by a magnetic field. Processes **9**(8), 1339 (2021)

40. K. Al-Farhany, M.F. Al-dawody, D.A. Hamzah, W. Al-Kouz, Z. Said, Numerical investigation of natural convection on Al$_2$O$_3$–water porous enclosure partially heated with two fins attached to its hot wall: under the MHD effects. Appl. Nanosci. **10**, 1–18 (2021)

41. N.A. Jabbar, S. Abdul Hussein, K. Al-Chlaihawi, Q. Al-anssari, L. Al-Ansari, CFD analysis of natural convection in a square cavity with two thin baffles of different lengths and positions on the vertical opposite walls. J. Mech. Eng. Res. Dev. **43**(3), 174–185 (2020)

42. L. Wang, W. Wang, Y. Cai, D. Liu, F. Zhao, Effects of porous fins on mixed convection and heat transfer mechanics in lid-driven cavities: full numerical modeling and parametric simulations. Transport Porous Media **132**, 495–534 (2020)

43. T. Tayebi, H.F. Öztop, A.J. Chamkha, Natural convection and entropy production in hybrid nanofluid filled-annular elliptical cavity with internal heat generation or absorption. Therm. Sci. Eng. Progress **19**, 100605 (2020)

44. Z. Li, A.K. Hussein, O. Younisd, M. Afrand, S. Feng, Natural convection and entropy generation of a nanofluid around a circular baffle inside an inclined square cavity under thermal radiation and magnetic field effects. Int. Commun. Heat Mass Transf. **116**(4),104650 (2020)

45. A. Alsabery, I. Hashim, A. Hajjar, M. Ghalambaz, S. Nadeem, P.M. Saffari, Entropy generation and natural convection flow of hybrid nanofluids in a partially divided wavy cavity including solid blocks. Energies (2020). https://doi.org/10.3390/en13112942

46. R.D.C. Oliveski, M.H. Macagnan, J.B. Copetti, Entropy generation and natural convection in rectangular cavities. Appl. Therm. Eng. **29**, 1417–1425 (2009)

47. A.I. Alsabery, T. Tayebi, A.J. Chamkha, I. Hashim, Effect of rotating solid cylinder on entropy generation and convective heat transfer in a wavy porous cavity heated from below. Int. Commun. Heat Mass Transf. **95**, 197–209 (2018)

48. F. Selimefendigil, H.F. Öztop, Effects of conductive curved partition and magnetic field on natural convection and entropy generation in an inclined cavity filled with nanofluid. Phys. A Stat. Mech. Appl. **540**, 123004 (2020)

49. A. Chamkha, M.A. Mansour, A.M. Rashad, H. Kargarsharifiabad, T. Armaghani, Magneto-hydrodynamic mixed convection and entropy analysis of nanofluid in gamma-shaped porous cavity. J. Thermophys. Heat Transf. **34**(4), 836–847 (2020)

50. M. Hashemi-Tilehnoee, A.S. Dogonchi, S.M. Seyyedi, A.J. Chamkha, D. D. Ganji, Magnetohydrodynamic natural convection and entropy generation analyses inside a nanofluid-filled incinerator-shaped porous cavity with wavy heater block. J. Therm. Anal. Calorim. **141**, 2033–2045 (2020)

51. M. Hashemi-Tilehnoee, A.S. Dogonchi, S.M. Seyyedi, M. Sharifpur, Magneto-fluid dynamic and second law analysis in a hot porous cavity filled by nanofluid and nano-encapsulated phase change material suspension with different layout of cooling channels. J. Energy Storage **31**, 101720 (2020)

52. S.M. Seyyedi, A.S. Dogonchi, D.D. Ganji, M. Hashemi-Tilehnoee, Entropy generation in a nanofluid-filled semi-annulus cavity by considering the shape of nanoparticles. J. Therm. Anal. Calorim. **138**(2), 1607–1621 (2019)

53. S. Shaw, A.S. Dogonchi, M.K. Nayak, O.D. Makinde, Impact of entropy generation and nonlinear thermal radiation on Darcy-Forchheimer flow of $MnFe_2O_4$-Casson/water nanofluid due to a rotating disk: application to brain dynamics. Arab. J. Sci. Eng. **45**(7), 5471–5490 (2020)

54. S.M. Seyyedi, A.S. Dogonchi, M. Hashemi-Tilehnoee, D.D. Ganji, A.J. Chamkha, Second law analysis of magneto-natural convection in a nanofluid filled wavy-hexagonal porous enclosure. Int. J. Num. Methods Heat Fluid Flow **30**(11), 4811–4836 (2020)

55. S.M. Seyyedi, A.S. Dogonchi, R. Nuraei, D.D. Ganji, M. Hashemi-Tilehnoee, Numerical analysis of entropy generation of a nanofluid in a semi-annulus porous enclosure with different nanoparticle shapes in the presence of a magnetic field. Eur. Phys. J. Plus **134**(6), 1–20 (2019)

56. A.S. Dogonchi, M.S. Sadeghi, M. Ghodrat, A.J. Chamkha, Y. Elmasry, R. Alsulami, Natural convection and entropy generation of a nano-liquid in a crown wavy cavity: effect of thermo-physical parameters and cavity shape. Case Stud. Thermal Eng. **27**, 101208 (2021)

57. M.S. Sadeghi, T. Tayebi, A.S. Dogonchi, M.K. Nayak, M. Waqas, Analysis of thermal behavior of magnetic buoyancy-driven flow in ferrofluid-filled wavy enclosure furnished with two circular cylinders. Int. Commun. Heat Mass Transf. **120**, 104951 (2021)

58. M. S. Sadeghi, A.S. Dogonchi, M. Ghodrat, A.J. Chamkha, H. Alhumade, N. Karimi, Natural convection of CuO-water nanofluid in a conventional oil/water separator cavity: application to combined-cycle power plants. J. Taiwan Inst. Chem. Eng. **124**, 307–319 (2021)

59. P. Gokulavani, M. Muthtamilselvan, B. Abdalla, Impact of injection/suction and entropy generation of the porous open cavity with the hybrid nanofluid. J. Thermal Anal. Calorim. **147**, 3299–3312 (2021)

60. S.M. Seyyedi, On the entropy generation for a porous enclosure subject to a magnetic field: different orientations of cardioid geometry. Int. Commun. Heat Mass Transf. **116**, 104712 (2020)

61. M. Hatami, L. Sun, D. Jing, H. Günerhan, P.K. Kameswaran, Rotating cylinder turbulator effect on the heat transfer of a nanofluid flow in a wavy divergent channel. J. Appl. Comput. Mech. **7**(4), 1987–1998 (2021)

62. M. Usman, Z.H. Khan, M.B. Liu, MHD natural convection and thermal control inside a cavity with obstacles under the radiation effects. Physica A **535**, 122443 (2019)

63. M.S. Sadeghi, T. Tayebi, A.S. Dogonchi, T. Armaghani, P. Talebizadehsardari, Analysis of hydrothermal characteristics of magnetic Al_2O_3-H_2O nanofluid within a novel wavy enclosure during natural convection process considering internal heat generation. Math. Methods Appl. Sci. **10**, 1–13 (2020)

64. M. Paroncini, F. Corvaro, Natural convection in a square enclosure with a hot source. Int. J. Therm. Sci. **48**(9), 1683–1695 (2009)

65. A.M. Aly, A. Al-Hanaya, Z. Raizah, The magnetic power on natural convection of NEPCM suspended in a porous annulus between a hexagonal-shaped cavity and dual curves. Case Stud. Therm. Eng. **28**, 101354 (2021)

66. H.F. Oztop, E. Abu-Nada, Y. Varol, A. Chamkha, Natural convection in wavy enclosures with volumetric heat sources. Int. J. Therm. Sci. **50**(4), 502–514 (2011)